# BEHAVIOURAL ANALYSIS OF THERMAL ACTUATOR MADE UP OF METALS LIKE TITANIUM, STAINLESS STEEL AND BRASS

by

THANGAMANI BALASUBRAMANIAN PRAVEEN BALAJI

Presented to the Faculty of the Graduate School of

The University of Texas at Arlington in Partial Fulfillment

of the Requirements

for the Degree of

MASTER OF SCIENCE IN ELECTRICAL ENGINEERING

THE UNIVERSITY OF TEXAS AT ARLINGTON

December 2011

Copyright © by THANGAMANI BALASUBRAMANIAN PRAVEEN BALAJI 2011

All Rights Reserved

ACKNOWLEDGEMENTS

First and foremost, I would like to express my sincere gratitude to my supervising professor, Dr. Chiao for his continuous support on my research, for his patience, motivation, enthusiasm, and immense knowledge. His guidance helped me in all the time of research and writing of this thesis.

I would also like to thank my thesis defense committee members, Dr. Davis and Dr. Dillon for their interest towards my research.

My sincere thanks to Mr. Hung Cao for his unconditional support and guidance and Mr. Matthew Oseng for helping me carry on my research work effectively. I am also thankful to my fellow lab mates in iMEMS group for providing me the best team environment.

Last but not the least; I would like to thank my family, my father Thangamani Balasubramanaian, my mother Latha Balasubramanian and my twin brother Balasubramanian Naveen for their everlasting unconditional love.

November 21, 2011

ABSTRACT

BEHAVIOURAL ANALYSIS OF THERMAL ACTUATOR MADE UP OF METALS LIKE TITANIUM, STAINLESS STEEL AND BRASS

Thangamani Balasubramanian Praveen Balaji, M.S.

The University of Texas at Arlington, 2011

Supervising Professor: Jung-Chih Chiao

Out of the various MEMS actuators, thermal actuators are easy to realize and creates more force by consuming less power compared with other types of MEMS based actuators [2 - 4].Conventional thermal actuators are made up of poly silicon which requires the use of costlier equipment's for its fabrication and further it has to go through dark room processing which is time consuming. In our system the thermal actuator are made up of metals like titanium, stainless steel and brass which were fabricated using a programmable 5-W 355-nm laser system, which makes the fabrication process cheaper and less time consuming. Performance of the actuator in terms of displacement and measured force also showed a marginal improvement when it is made up of metal. In our work we designed a system that uses a U-beam thermal actuator otherwise called as pseudo bimorph made up of three different metals. We studied and determined the behavior of the metal thermal actuator with respect to their displacement and force generated, and also determined the best design profile of thermal actuator based on varying their design parameters and by performing simulation using ANSYS. The obtained simulation data was also been validated against the experimental data. Finally a comparative analysis was made between the three metal thermal actuators.

TABLE OF CONTENTS

LIST OF ILLUSTRATIONS

LIST OF TABLES

# CHAPTER 1

# INTRODUCTION

## 1.1 Background about MEMS Based Thermal Actuators

MEMS actuation can be achieved through various methods and once such traditionally used method to achieve it was by using thermal actuators, which are known to produce large magnitude of force at lesser actuation voltage [9]. The thermal actuator achieves motion through thermal expansion that occurs due to Joule heating [7]. In general there are two commonly used thermal actuators which are used to produce in-plane actuation, they are “U” shaped and “V” shaped thermal actuator [4].

## 1.2 Motivation

Conventional MEMS based thermal actuators are made up of poly silicon which requires time and cost consuming dark room processing for their fabrication and further its performance are limited by its current range it can work with but all these odds of poly silicon thermal actuator can be overcome by the metal thermal actuator. Thereby in this research we designed, optimized, fabricated, tested and analyzed the thermal actuators made up of metals like titanium, stainless steel and brass so as to determine and compare their overall performance with respect to displacement and the force produced by each of them.

## 1.3 Working Principle of Thermal Actuator

The U-beam thermal actuator in general consists of three main parts a hot arm, a cold arm and a flexure arm, Fig 1.1 describes the parts in the thermal actuator. The hot arm has lesser cross sectional area and are much thinner compared to the cold arm so the hot arm are much more electrically resistive compared to the cold arm [1]. The cold arm and the hot arm are connected together at one of their ends and each of their other ends is connected to a contact pad which will be then be anchored to the substrate. The thermal actuator works on the

principle of Joule heating, whenever the thermal actuator was actuated by passing current through it, the hot arm which are electrically more resistive gets heated up more compared to the much less resistive cold arm. The thermal expansion of hot arm results in the increase in length of the hot arm since one end of the hot arm was anchored to the substrate with the help of the contact pad much of the expansion in hot arm length will be focused at the end where it is connected with the cold arm [6]. The thermal expansion of the hot arm constrained by the cold arm together with the freedom of bending provided by the flexure arm results in the movement of thermal actuator in an arc like fashion. The U - beam thermal actuator thus produces a arc like motion but when several of thermal actuators are connected in an array by joining all their tips through a yoke then it can be forced to produce a linear motion.

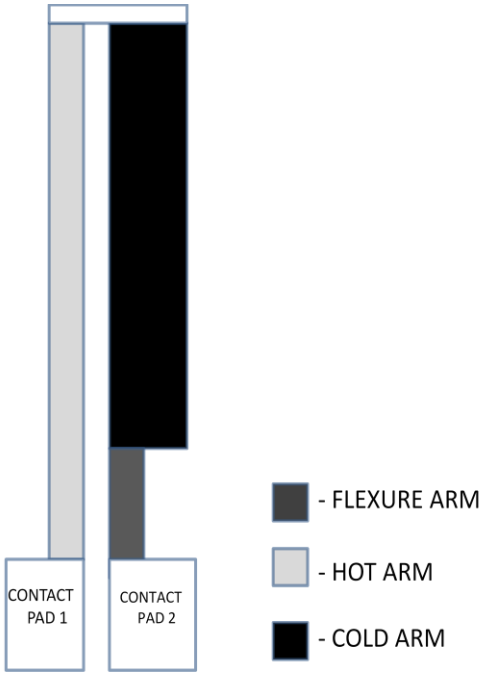


Figure 1.1 Parts of U-beam thermal actuator

In our design of metal thermal actuator, we kept cold arm width, hot arm width and total actuator length constant but varied the flexure arm length so as to determine the best actuator design profile based on their behavior with respect to displacement and force produced by each of them, Figure 1.2 describes the design parameters of the thermal actuator. We only varied the

flexure arm length as a percentage of total length which are 6% 7%, 8%, 10%, 20%, 30% and 40% .The thickness of the three commercially available metals titanium, stainless steel and brass we used are 127 micro meter. The figure shown below describes the dimension of the thermal actuator, where Lc represents the cold arm length, Lct represents the flexure arm length, Lj represents the length of the joint that connects hot arm with the cold arm, Wc represents the cold arm width that was assigned to be 1000 micro meter, Wh represents hot arm width that was assigned to be 200 micro meter and G represents the width of the gap between the hot and the cold arm, G was assigned to be 200 micro meter. The dimension of the contact pad was 1000 micro meter by 1000 micro meter.

The table 1.1 represents the various percentages of flexure arm length to the total actuator length used for our behavioral study and the total actuator length was assigned to be 10000 micro meter and was kept constant.

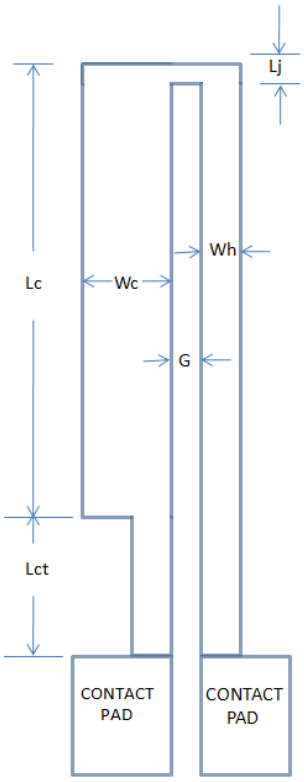


Figure 1.2 Design parameters of thermal actuator structure.

Table 1.1 Percentage ratio of flexure arm length to the total length of thermal actuator

| [Lct/(Lc+Lct)]100% | Lc(micro meter) | Lct(micro meter) |
|---|---|---|
| 6% | 9400 | 600 |
| 7% | 9300 | 700 |
| 8% | 9200 | 800 |
| 10% | 9000 | 1000 |
| 20% | 8000 | 2000 |
| 30% | 7000 | 3000 |
| 40% | 6000 | 4000 |

## 1.4 Simulation in ANSYS

In ANSYS, we carried out coupled field analysis wherein the thermal, electrical and structural analysis are coupled together and through this analysis the displacement, force and the temperature profile of the actuator can be determined.

The table 1.2, 1.3 and 1.4 describes the material properties of Titanium, Stainless steel and Brass that have to be fed as input parameters in ANSYS depending upon the metal with which the thermal actuator was made up of.

Table 1.2 Material Properties of Titanium

| Material properties | Corresponding value | Units in terms of ANSYS measurement scale(μMKSV) |
|---|---|---|
| Young's modulus | 103 x$10^3$ | Mpa |
| Poisson's ratio | 0.347(no unit) | no unit |
| Thermal conductivity | 19.9 x$10^6$ | pW/um-K |
| Thermal expansion | 8.6 x $10^{-6}$ | /K |
| Resistivity | 560 x$10^{-15}$ | tera ohm-um |

Table 1.3 Material Properties of Stainless steel

| Material properties | Corresponding value | Units in terms of ANSYS measurement scale(μMKSV) |
|---|---|---|
| Young's modulus | 193x10³ | Mpa |
| Poisson's ratio | 0.3 | no unit |
| Thermal conductivity | 16.3 x$10^{6}$ | pW/um-K |
| Thermal expansion | 17x$10^{-6}$ | /K |
| Resistivity | 720x$10^{-15}$ | tera ohm-um |

Table 1.4 Material Properties of Brass

| Material properties | Corresponding value | Units in terms of ANSYS measurement scale(μMKSV) |
|---|---|---|
| Young's modulus | 117 x10³ | Mpa |
| Poisson's ratio | 0.35(no unit) | no unit |
| Thermal conductivity | 120 x$10^{6}$ | pW/um-K |
| Thermal expansion | 20 x $10^{-6}$ | /K |
| Resistivity | 62 x$10^{-15}$ | tera ohm-um |

The thermal actuator structure with required dimension was modeled using blocks in ANSYS and the individual blocks are finally glued together so as to make it all a single structure, the element type for the model created was defined to be SOLID98 so as to carry on thermal and electrical analysis .The material properties corresponding to the metal with which the actuator was made up of was assigned to the thermal actuator structure by meshing. Finally, the required boundary condition was set up and the simulation was carried on with the applied boundary conditions. The obtained results are then tabulated to carry on further analysis. Figure 1.2 describes the thermal actuator created using blocks and Figure 1.3 describes the thermal actuator meshed with the desired material properties.

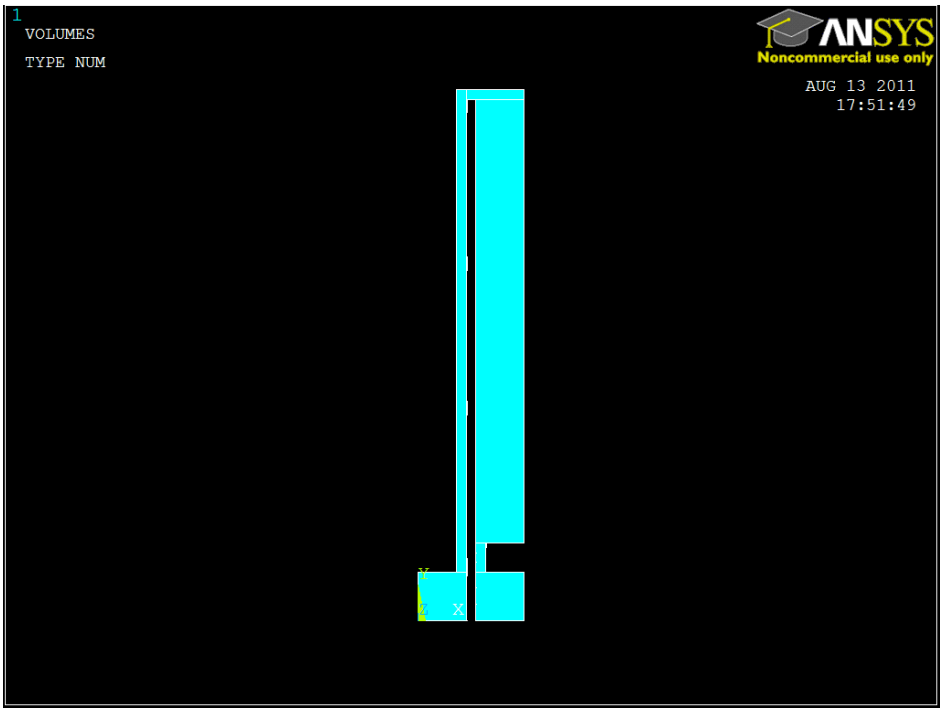


Figure 1.3 Thermal actuator structure using blocks in ANSYS.

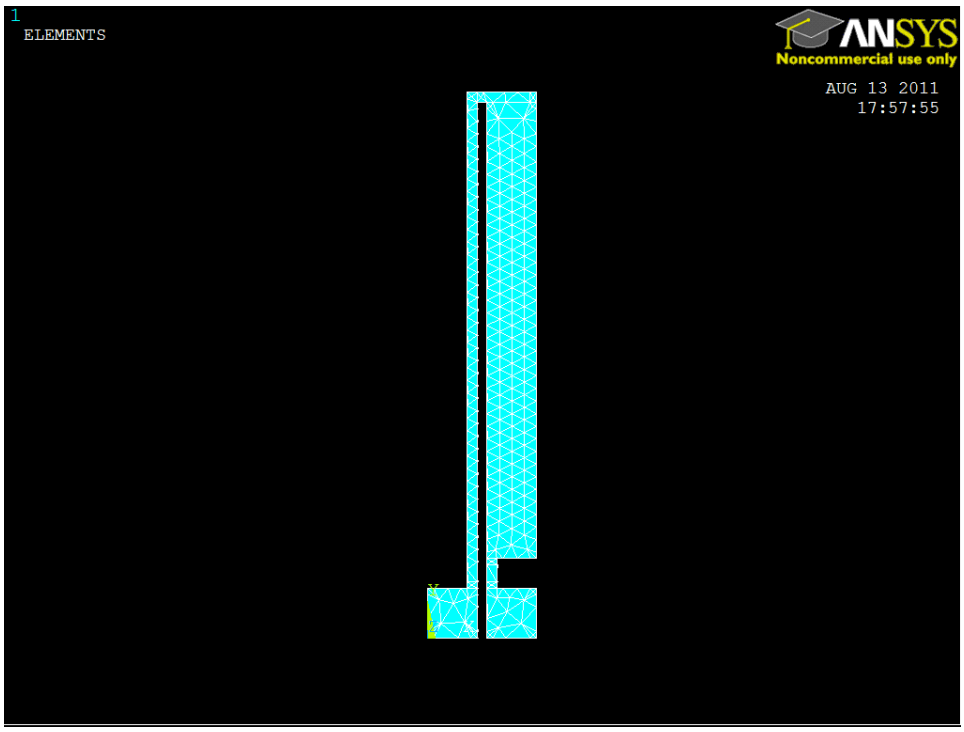


Figure 1.4 Meshing of thermal actuator structure in ANSYS.

## 1.5 Laser Micromachining

In Laser micromachining technique, a programmable 5-W 355-nm laser system was used. The required metal cut out design was then done using an *Oxford diode laser*. On the software side, the needed thermal actuator design with the required dimension was sketched using a software called '*Alphacam Advanced profiling'*. The software then generates an output program that defines the cut path as per the design. This output program was then loaded into the laser machine through the computer interface provided by its manufacturer. Laser settings such as laser power, the number of loops for the laser to follow a cut path, laser speed and the vertical distance between the metal sheet and the laser could be changed as per the metal on which the cut outs are to be made. On the hardware side, the needed metal sheet on which the cut outs are to be made was clamped on to the laser machine's workbench and once the metal sheets were fixed, the laser will then be activated by opening the laser shutter and by turning on the laser, the Figure 1.5 below shows the *Oxford laser* which was used to make the metal thermal actuators cut outs.


Figure 1.5 Oxford laser machine.

## 1.6 Document Organization

The body of this thesis composes of three main parts which are found in Chapters 2, 3 and 4. Chapter 2 describes the displacement produced by the thermal actuators made up of three different metals which are Titanium, Stainless steel and Brass. Chapter 3 describes the maximum temperature of the thermal actuator's hot arm on actuation. Chapter 4 describes the force produced by the thermal actuators under loaded and unloaded conditions. The results in both Chapters 2 and 4 are drawn through simulation and also through experimentation; the obtained results are then validated and compared so as to determine the best of the three thermal actuators made up of Titanium, Stainless steel and Brass which will be discussed in the final chapter.

# CHAPTER 2

# DISPLACEMENT MEASUREMENT OF THERMAL ACTUATOR

## 2.1 Introduction

The thermal actuators are known for their large magnitude of displacement produced. The displacement magnitude produced by the U-beam thermal actuators depends much on the hot arm width and flexure arm length [1]. The hot arm width plays an important factor since when the hot arm width decreases, its cross sectional area also decreases resulting in increase of overall electrical resistance of the hot arm, which results in increase of temperature difference between the cold arm and hot arm when current was passed through the thermal actuator resulting in increase in displacement value compared to the thicker hot arm. Perhaps there is a limitation on how thin the hot arm can be made due to the fact that the hot arm melts because of high temperature resulting from high resistance during actuation.

In our design, the hot arm width was kept at a constant value of 200 micro meters, the magnitude of thermal actuator's tip displacement at a given constant input current now becomes dependent on the percentage of flexure arm length to the total length. We know that the flexure arm of thermal actuator helps in bending of the thermal actuator and hence if the flexure arm length was zero, the thermal actuator on actuation produces zero displacement ideally but if the flexure arm length was same as the total actuator length then it behaves like the hot arm and thus it expands and impedes the force produced by hot arm on generating an equally opposite force due to thermal expansion resulting in zero actuator displacement ideally, in between the two extreme cases mentioned above the actuator's tip displacement follows a bell shaped curve with respect to varying flexure arm length provided the total actuator length was kept constant. In short, the plot for flexure arm length Versus the actuator displacement at a fixed total actuator

length follows a bell shaped curve and our objective was to find the peak value in the curve [1]. Thus an effective tradeoff was needed so as to determine the suitable length of the flexure arm at which displacement magnitude produced by the thermal actuator's tip was much higher by varying flexure arm length as a percentage of total thermal actuator length.

## 2.2 Simulation Method

### *2.2.1. Modeling and Simulation of Thermal Actuator*

The thermal actuator of the required dimension was modeled in ANSYS using blocks and the required material data was assigned to the created thermal actuator model according to the metal with which the thermal actuator was made up of. The simulation was carried out separately for the actuator made up of brass, titanium and stainless steel. We varied the flexure arm length as a percentage of total length, which are 6% 7%, 8%, 10%, 20%, 30% and 40% by keeping the total actuator length constant. For each of the percentage mentioned above, the maximum displacement produced by the actuator was noted by varying the current input to the actuator from 0.25 A to 1.25 A in steps of 0.25 A.

Applied boundary conditions in ANSYS for carrying out displacement measurement

1. The contact pads are anchored i.e. the degree of freedom was made zero in all three dimensions.
2. The contact pads temperatures are maintained at 30 degree Celsius.
3. The required voltage was applied across the contact pads to actuate the thermal actuator.

The X-displacement profile of the thermal actuator was determined to find the maximum horizontal displacement produced by the actuator during actuation, the figure shown bellow represents the X-displacement profile of the thermal actuator and the color scale at the bottom of the figure represents the displacement range the actuator undergone on actuation in a VIBGYOR color pattern with the violet color representing the region of minimum displacement and the red color representing the region of maximum displacement. We can observe from

figure 2.1 that the maximum displacement occurs at the top right corner of the cold arm since the actuator displaces in the direction towards cold arm in a curved path on actuation, the maximum displacement as shown in the scale at the bottom was tabulated to be considered the maximum displacement produced by the thermal actuator.

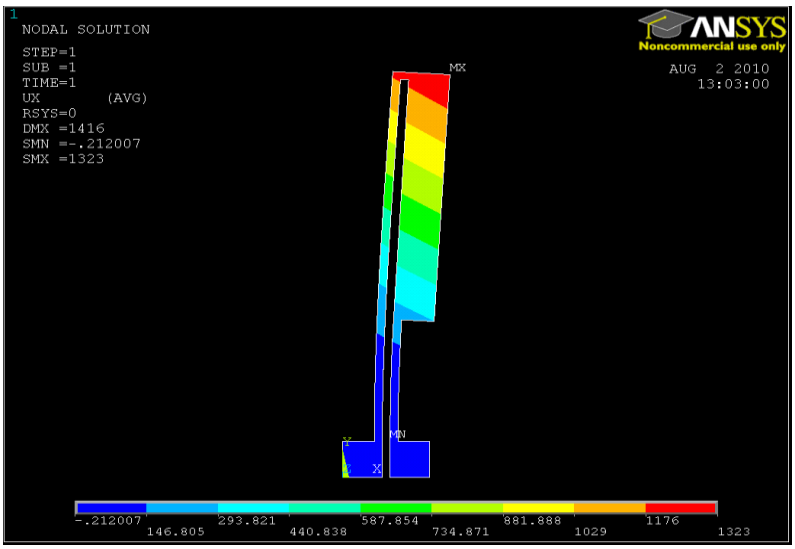


Figure 2.1 X-Displacement profile of thermal actuator.

*2.2.2. Simulation Results*

We can observe from figure 2.2 that for an actuator with the fixed percentage of flexure arm length to the total length, the displacement produced by the actuator increases with the increase in current input since the temperature difference between the hot arm and cold increases with the increase in input current magnitude and hence the displacement value also increases. The actuator displacement and the input current follow a non linear relationship due to the non linear dependence of current with temperature as from Joule's law of heating [7]. As we go from 6%, 7%, 8% and 10% thermal actuators made up of same metal at a constant actuator input current of 1.25 A, we can observe from figure 2.3 that the plot of flexure arm length Versus maximum horizontal actuator displacement follows a bell shaped curve at a constant actuator input current of 1.25 A. The flexure arm length for which the actuator displacement reaches maximum was found to be 7% for thermal actuator made up titanium,

stainless steel and also brass. The actuator tip displacement for 6%, 7% and 8% for all the three metal type thermal actuators are fairly distinguishable hence we have listed the tip displacement for 6%, 7% and 8% Titanium, Stainless steel and Brass actuators in table 2.1, 2.2 and 2.3 respectively.

Table 2.1 Tip displacement of Titanium thermal actuator

| Current (Ampere) | 6% Maximum actuator tip displacement (micro meters) | 7% Maximum actuator tip displacement (micro meters) | 8% Maximum actuator tip displacement (micro meters) |
|---|---|---|---|
| 0 | 0 | 0 | 0 |
| 0.25 | 19.867 | 19.983 | 19.958 |
| 0.5 | 78.705 | 79.166 | 79.061 |
| 0.75 | 176.768 | 177.804 | 177.566 |
| 1 | 314.055 | 315.898 | 315.473 |
| 1.25 | 490.568 | 493.446 | 492.781 |

Table 2.2 Tip displacement of Stainless steel thermal actuator

| Current (Ampere) | 6% Maximum actuator tip displacement (micro meters) | 7% Maximum actuator tip displacement (micro meters) | 8% Maximum actuator tip displacement (micro meters) |
|---|---|---|---|
| 0 | 0 | 0 | 0 |
| 0.25 | 61.41 | 61.761 | 61.671 |
| 0.5 | 244.124 | 245.526 | 245.156 |
| 0.75 | 548.647 | 551.801 | 550.964 |
| 1 | 974.98 | 980.586 | 979.095 |
| 1.25 | 1523 | 1532 | 1530 |

Table 2.3 Tip displacement of Brass thermal actuator

| Current (Ampere) | 6% Maximum actuator tip displacement (micro meters) | 7% Maximum actuator tip displacement (micro meters) | 8% Maximum actuator tip displacement (micro meters) |
|---|---|---|---|
| 0 | 0 | 0 | 0 |
| 0.25 | 1.43 | 1.437 | 1.439 |
| 0.5 | 3.942 | 3.964 | 3.963 |
| 0.75 | 8.129 | 8.175 | 8.168 |
| 1 | 13.991 | 14.071 | 14.056 |
| 1.25 | 21.527 | 21.652 | 21.626 |

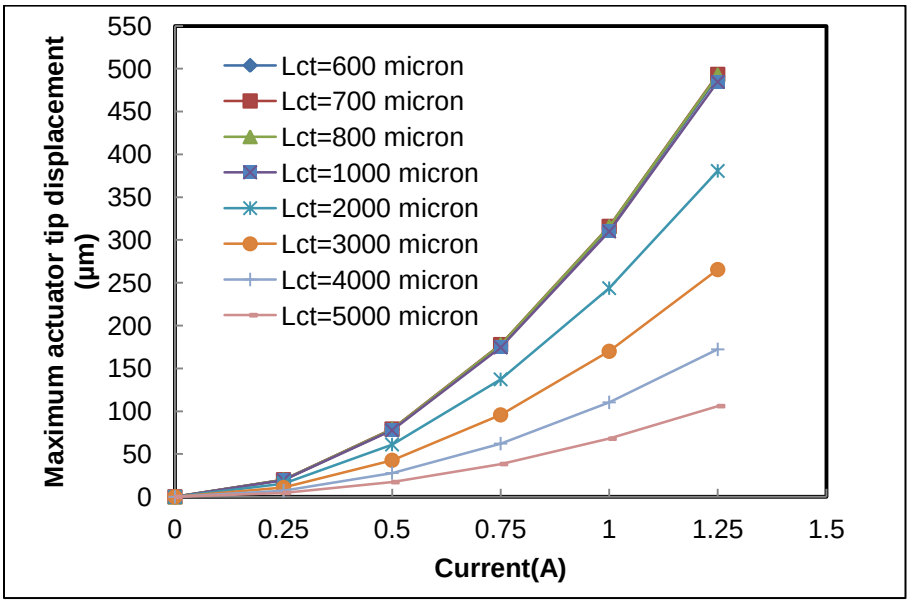


Figure 2.2 Tip displacement of titanium thermal actuator.

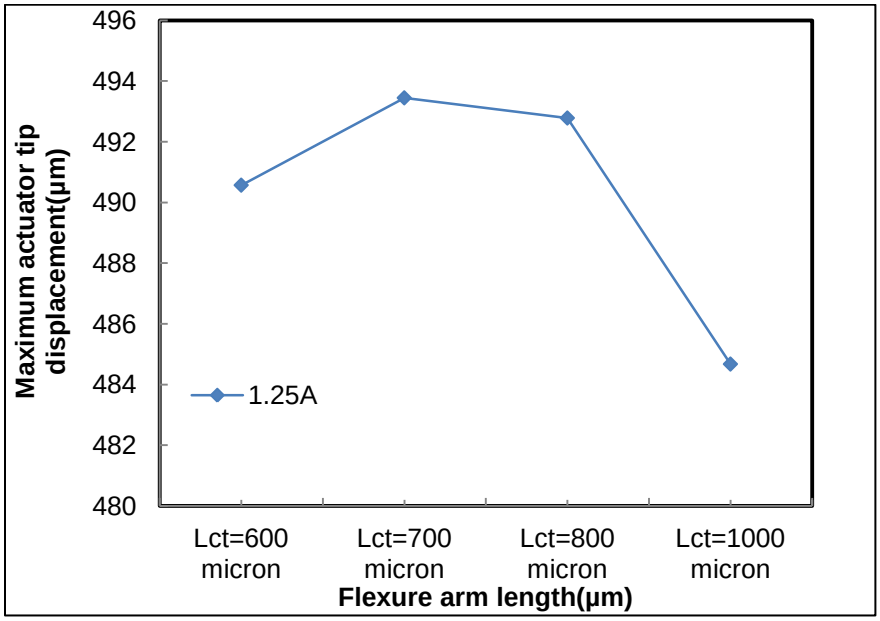


Figure 2.3 Actuator tip displacement Versus flexure arm length for Titanium thermal actuator at 1.25 A, the total actuator length at a constant value of 10000 micro meter.

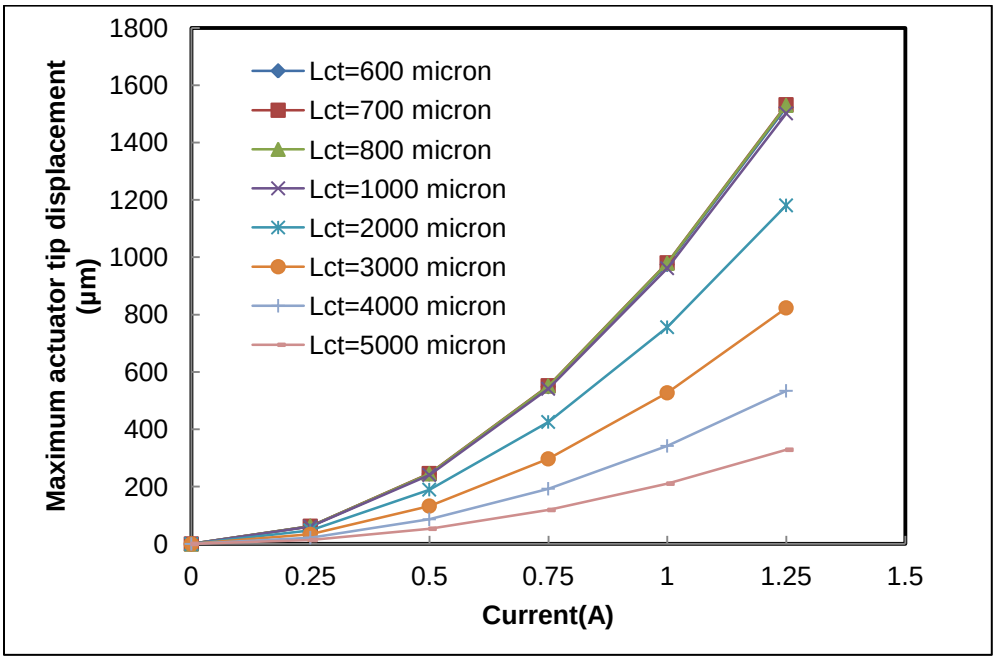


Figure 2.4 Tip displacement of stainless steel thermal actuator.

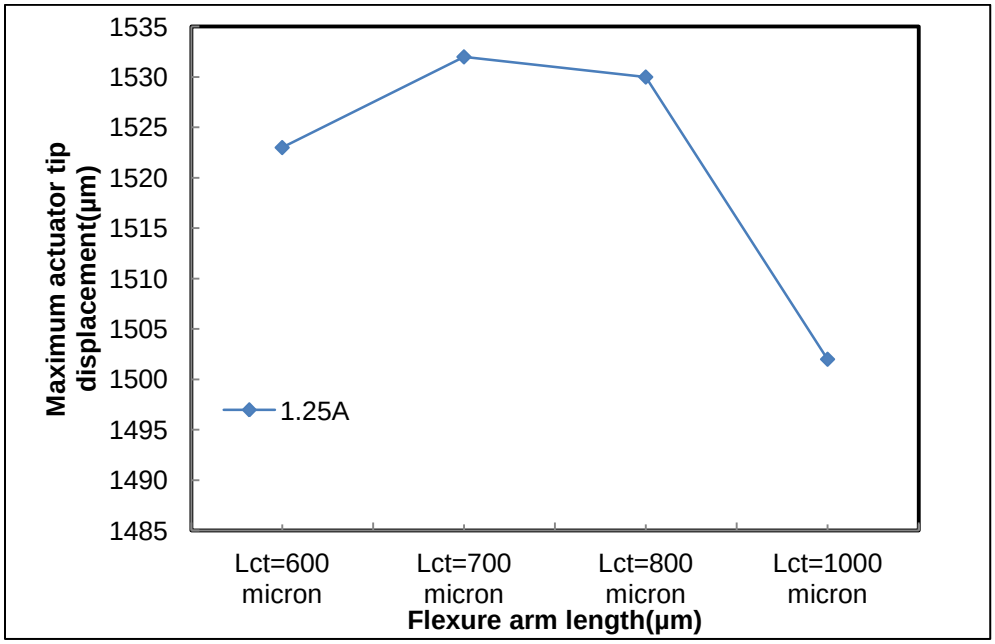


Figure 2.5 Actuator tip displacement Versus flexure arm length for stainless steel thermal actuator at 1.25 A, the total actuator length at a constant value of 10000 micro meter.

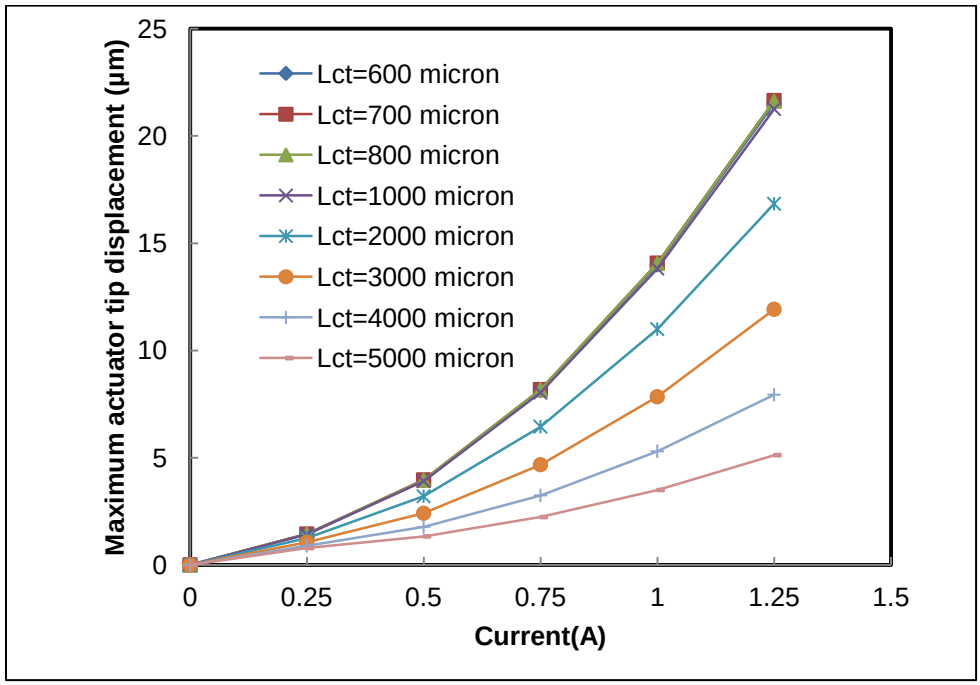


Figure 2.6 Tip displacement of brass thermal actuator.

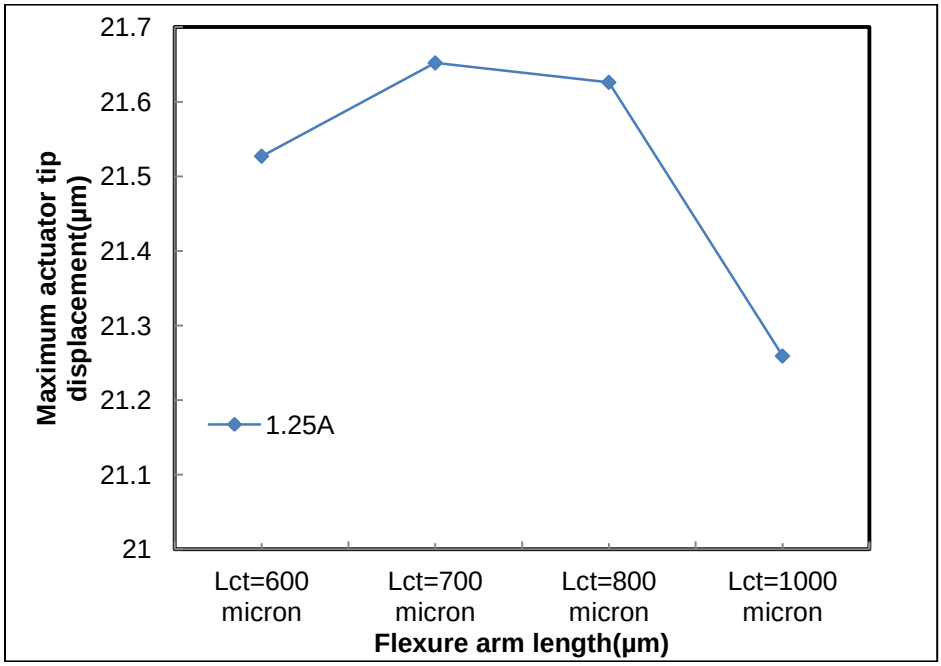


Figure 2.7 Actuator tip displacement Versus flexure arm length for brass thermal actuator at 1.25 A, the total actuator length at a constant value of 10000 micro meter.

## 2.3 Experimental Method

### *2.3.1. Modeling of Thermal Actuator*

The thermal actuator with the required dimension was created using the CAD design tool and the CAD design file was fed as input into the laser micro machine. In the laser micro machine, depending upon the required metal thermal actuator corresponding metal plate was kept inside the laser micro machine. The metal plates used for laser micromachining are generally coated with a photo-resist layer. For getting out titanium thermal actuator, a titanium metal plate was kept inside the laser micro machine. The thermal actuator design made using the CAD tool will be now used as the input reference to guide the movable laser, which then makes the required laser cut outs on the metal plate.

After laser micromachining the thermal actuator cut outs are removed from the base metal plates and are put inside a beaker filled with acetone and then the beaker containing the thermal actuator cutouts in acetone solution was subjected to ultrasonic mixing for about 10 minutes to remove the photo-resist layer on the cut outs. The thermal actuator cut outs are then dried up by exposing it to ambient air. A glass slide was used as a substrate over which the thermal actuator contact pads are anchored using silver epoxy. Figure 2.8 shown below represents the U – beam titanium thermal actuator.

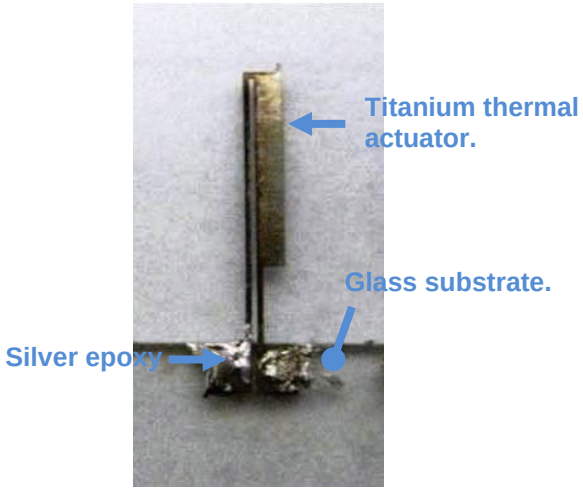


Figure 2.8 Titanium U-beam thermal actuator.

*2.3.2 Experimental Setup*

A custom designed probe was used to establish connection of current source with the contact pads of the thermal actuator; Figure 2.9 shows the custom designed probe and its connection with the thermal actuator. A multi-meter was then used to check the connectivity of the custom designed probe with the contact pads of the thermal actuator. A current source was then connected to the custom designed probe so as to actuate the thermal actuator. The thermal actuator in the glass substrate along with the custom designed probe was kept on the work bench of the video microscope. The workbench was movable so it was adjusted so as to get the clear view of actuator through the video microscope.

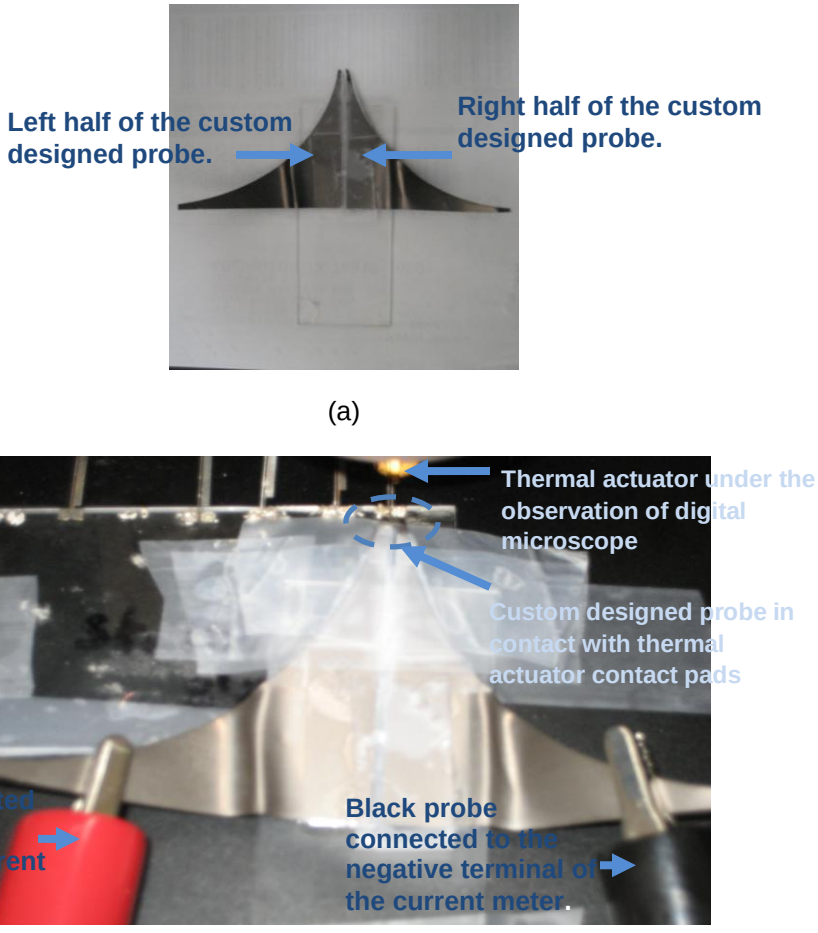


Figure 2.9 Probe (a) Top view and (b) connection of probe with thermal actuator.

The thermal actuator for which the displacement was to be measured was kept under the video microscope as shown in figure 2.10 and was excited with current starting from 0.25 A to 1.25 A in steps of 0.25 A. The actuator tip displacement was noted for each step in value of current by looking at the video output of the microscope and then by using the measurement scale provided as a software tool by the video microscope makers. The software measurement scale was set in accordance with the lens magnification factor and was used to measure the distance between two points. A reference mark was made on video screen that displays the unexcited thermal actuator so as to represent the top right most tip of the thermal actuator and then after current excitation another reference mark was made to denote the displaced position of the actuator tip, finally the distance between the two reference marks gives the needed actuator tip displacement.

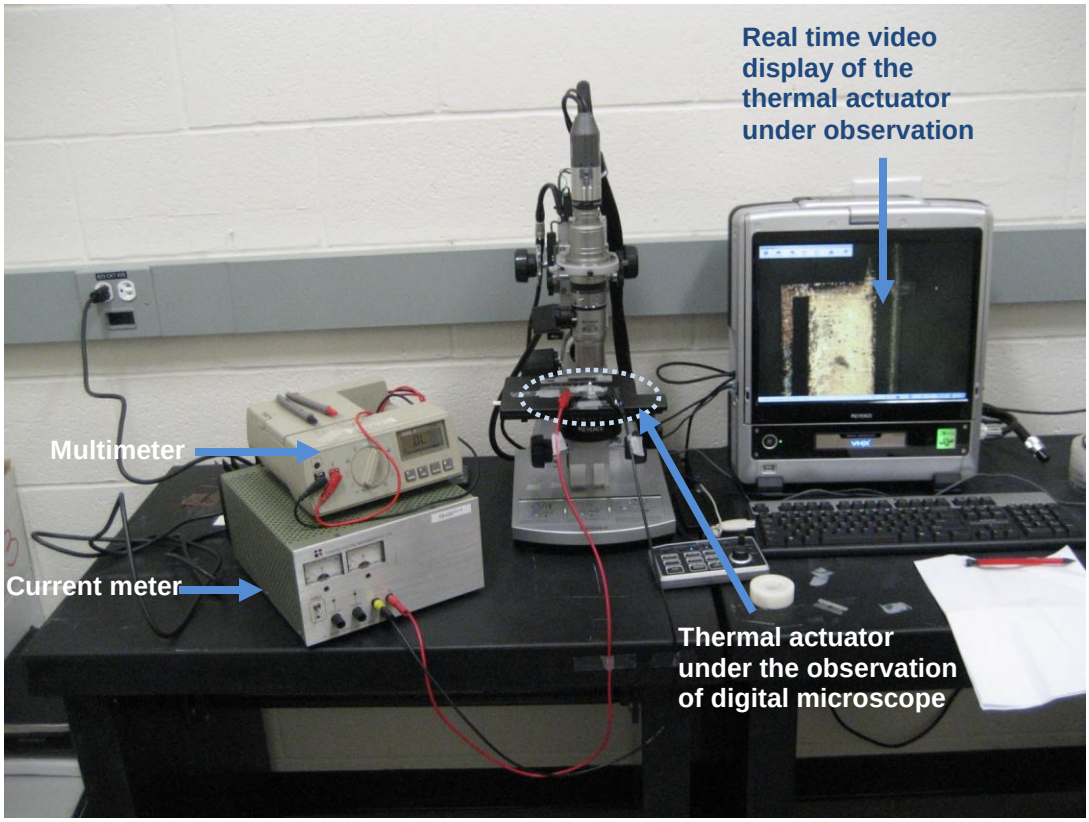


Figure 2.10 Experimental setup for measuring thermal actuator's displacement.

*2.3.3 Experimental Results*

The displacement was measured for 6%, 7%, 8%, 10%, 20%, 30% and 40% thermal actuators made up of metals like titanium, stainless steel and brass by exciting each of them with current ranging from 0.25 A to 1.25 A in steps of 0.25 A. The experimentally obtained displacement value was then plotted against the displacement value obtained through simulation in ANSYS so as to validate the experimental data with the simulation data.

We can observe from figure 2.11 and 2.12 that for titanium thermal actuators, simulation data and the experimental data almost match as we go from 6% all the way through 20% and at 30% and 40% the displacement value obtained from experiment surpasses the displacement value obtained from simulation, the reason behind this was partly because of the non uniform flat surface of the base metal plate used for making thermal actuators cut outs during laser micro machining, which results in the change in dimension of the laser micro machined thermal actuator from its expected dimension hence we can observe the width of the thermal actuator hot arm to be less than its expected width of 200 micro meter. The reduced hot arm width thus results in the increase in overall electrical resistance of the thermal actuator which in turn increases the displacement magnitude on actuation during experimentation [1].

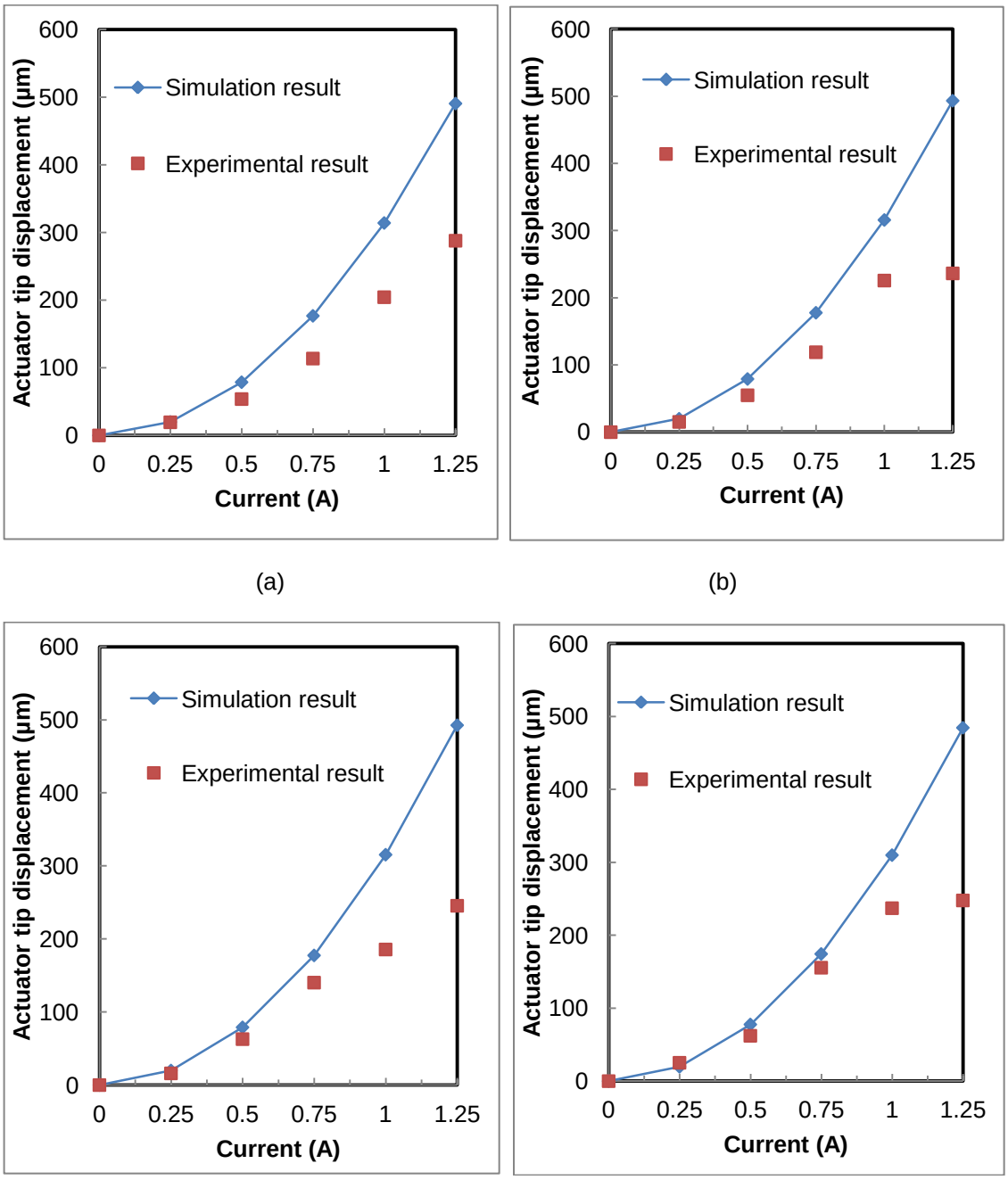


Figure 2.11 Titanium actuator tip displacement (a) 6% (b) 7% (c) 8% (d) 10%.

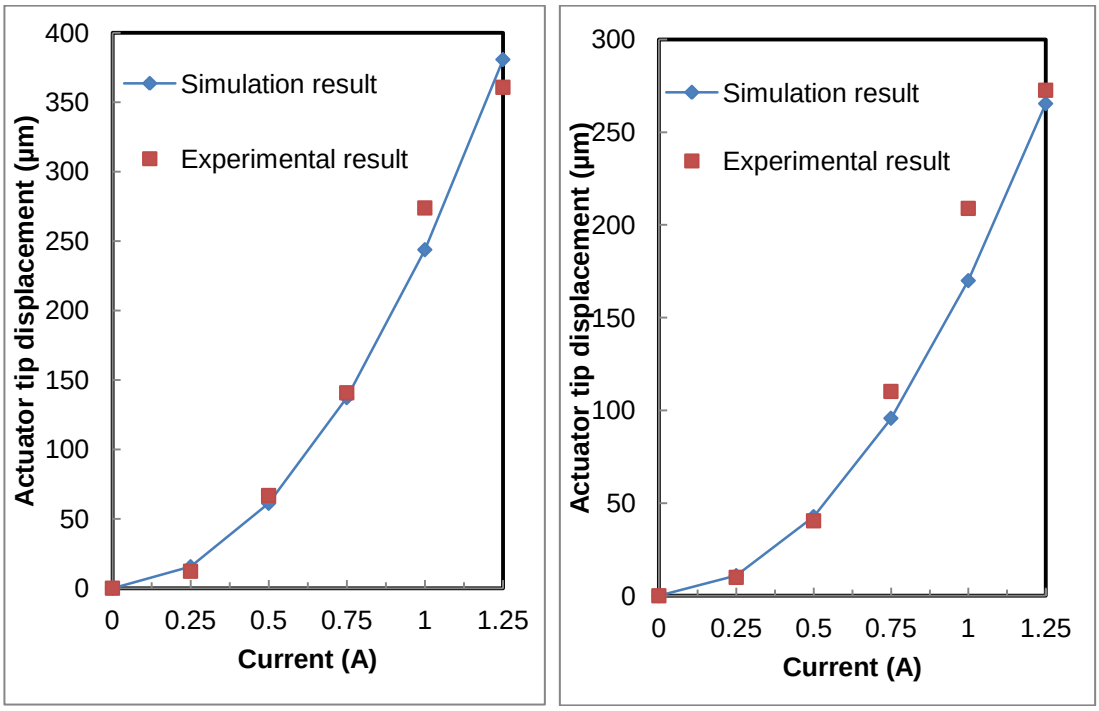


(a)




(b)

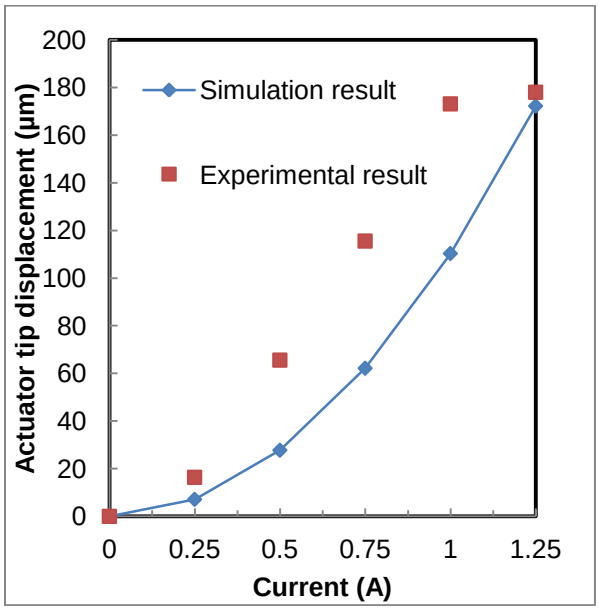


(c)

Figure 2.12 Titanium actuator tip displacement (a) 20% (b) 30% and (c) 40%.

We can observe from figure 2.13 and 2.14 that for stainless steel thermal actuators, the displacement value obtained through experiment was found to be far less than the expected value obtained from simulation. As we can observe from 6% all way through 40% at a current value of 0.25 A, the actuator's tip displacement value obtained through experiment and simulation does not differ much but as the current increases beyond it, the difference becomes much more amplified. Since the hot arm temperature of stainless becomes very much higher as we increase the current, which results in the enormous increase in displacement magnitude for each step in current value hence under such circumstances even a slight deformity in thermal actuator shape and dimension can result in affecting the thermal actuator behavior further the fact that assigned material properties for stainless steel for conducting simulation and the actual material properties of the stainless steel metal from manufacturers may not be the exactly same and are subjected to variation. We even determined the vertical displacement produced by the thermal actuator so as to determine whether the increase in vertical displacement could be the reason behind the decrease in horizontal displacement produced by the stainless thermal actuator.

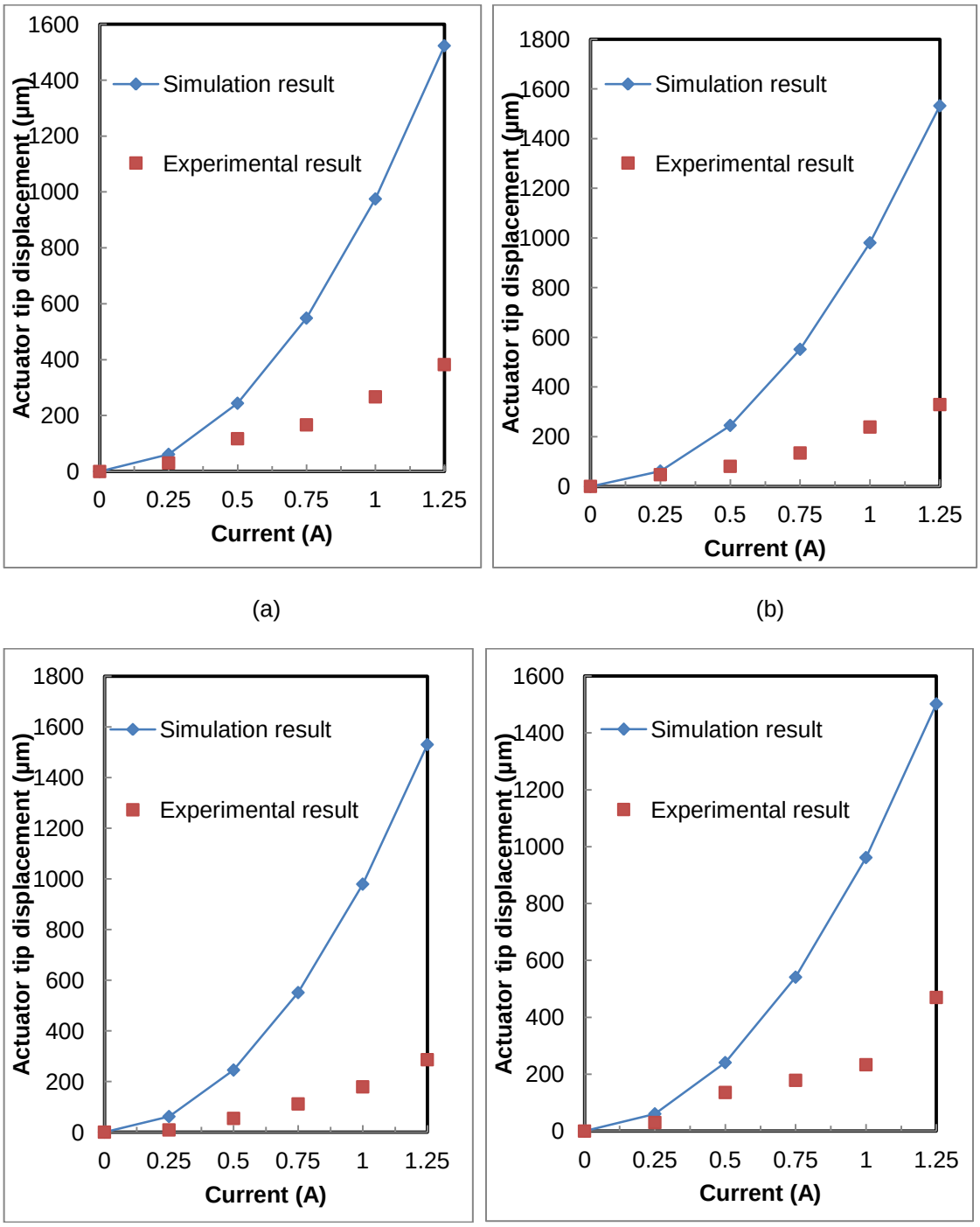


Figure 2.13 Stainless steel actuator tip displacement (a) 6% (b) 7% (c) 8% (d) 10%.

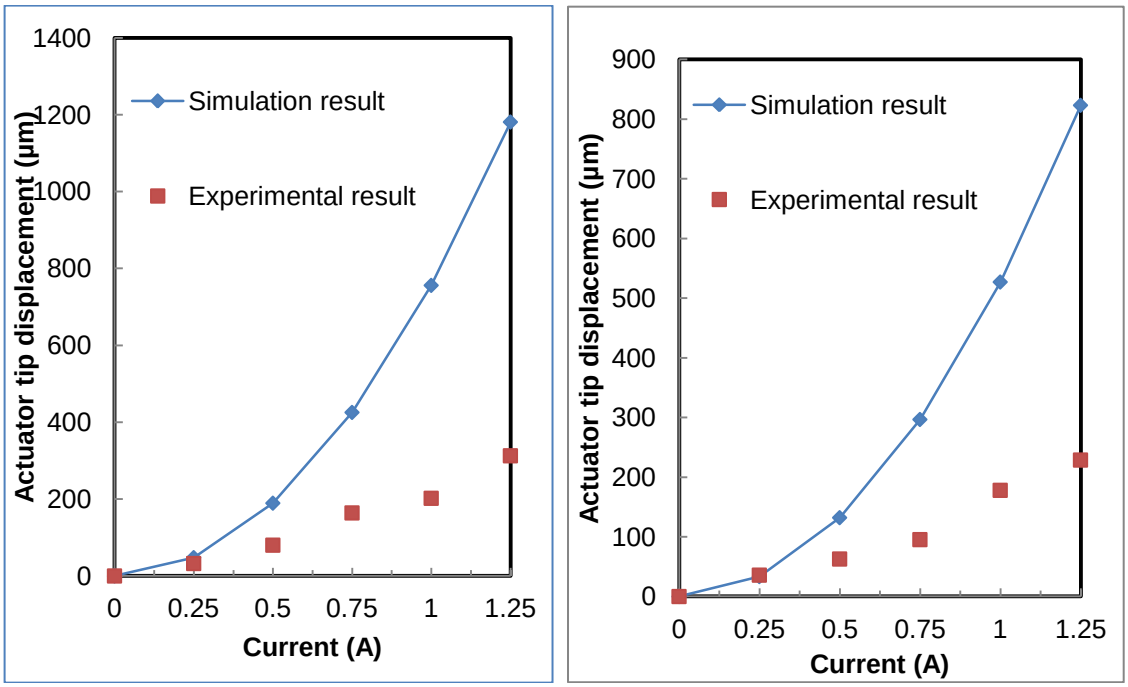


(a) (b)

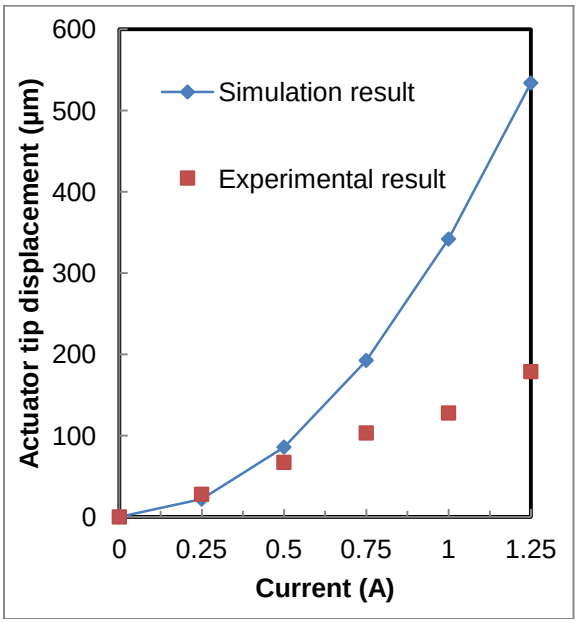


(c)

Figure 2.14 Stainless steel actuator tip displacement (a) 20% (b) 30% and (c) 40%.

We can observe from figure 2.15, 2.16 and 2.17 that for brass thermal actuators, the displacement value obtained from experiment becomes much higher than the simulation data as we go from 6% all way through to 40%. The reason was due to the reduced hot arm width of the thermal actuator obtained after laser micromachining and also due to the fact that assigned material properties for brass for conducting simulation and the actual material properties of the brass metal from manufacturers may not be the exactly same and are subjected to variation, which may be the cause for the difference in displacement data as observed.

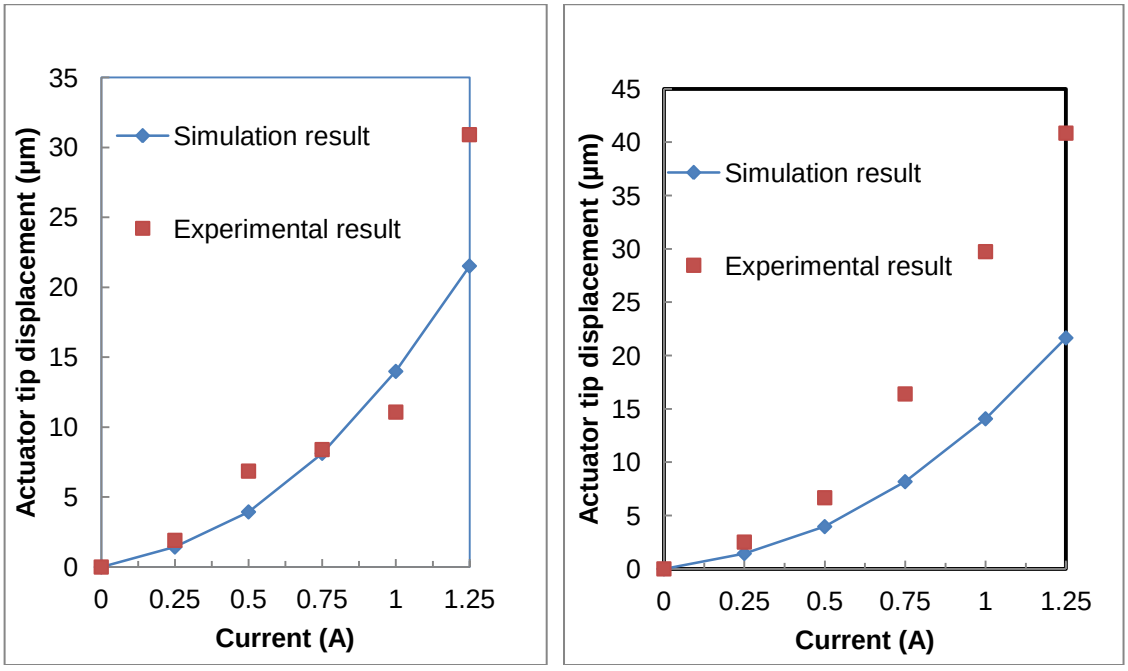


(a) (b)

Figure 2.15 Brass actuator tip displacement (a) 6% (b) 7%.

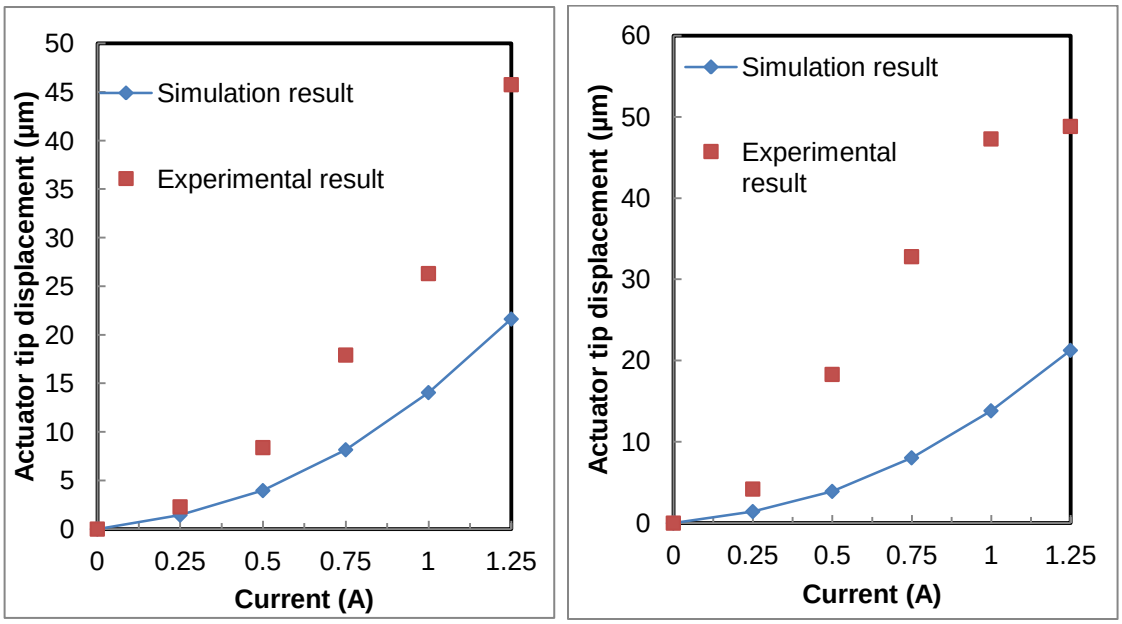


(a)




(b)

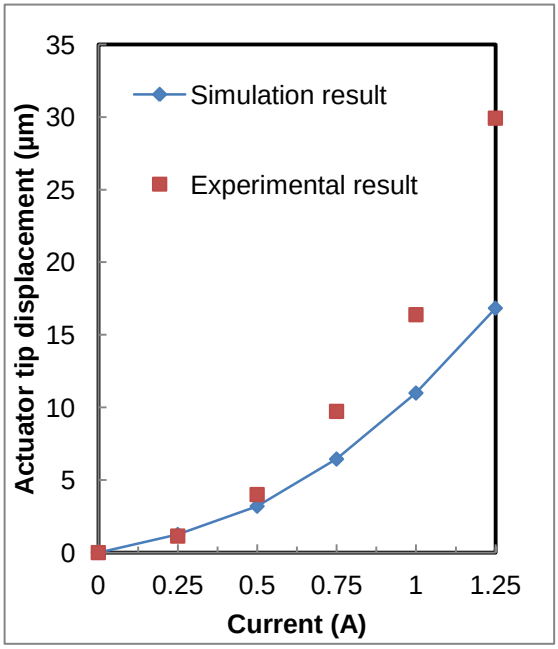


(c)

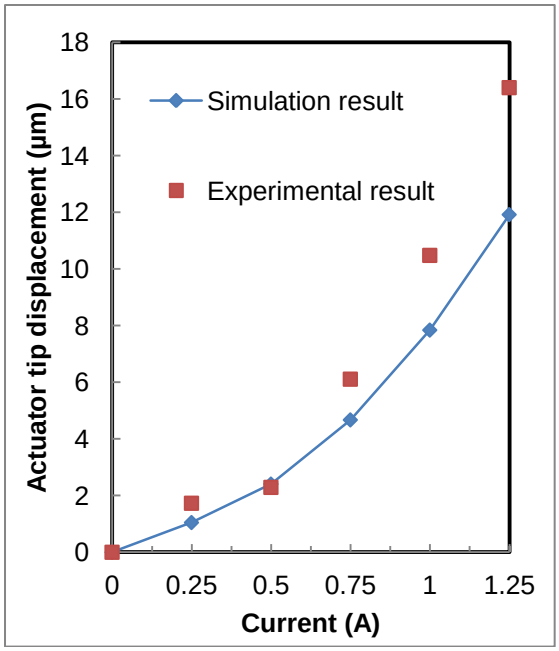


(d)

Figure 2.16 Brass actuator tip displacement (a) 8% (b) 10% (c) 20% (d) 30%.

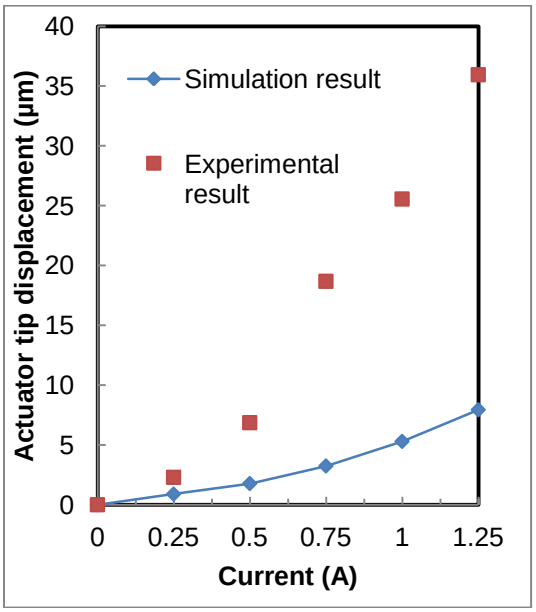


Figure 2.17 Brass actuator tip displacement 40%.

## 2.4 Conclusion

Since we found 7% thermal actuator gives the maximum displacement magnitude when it is made up titanium, stainless steel and brass, on the plot of the current versus displacement for thermal actuators made up of titanium, stainless steel and brass, we can say that the stainless steel thermal actuator produces much more displacement compared to titanium and brass thermal actuators but the displacement is one such behavior to characterize the thermal actuator as best for the working current range and force produced also plays a major part.

# CHAPTER 3

# HOT ARM TEMPERATURE OF THERMAL ACTUATOR

## 3.1 Introduction

The hot arm plays an important role in determining the behavior of the thermal actuator. The thermal expansion of the hot arm controls the actuator displacement and also the force produced by it. The hot arm thermal expansion is directly proportional to the hot arm temperature, which in turn is proportional to the actuator input current. As the input current magnitude increases, the hot arm temperature also increases however there is a limitation on it depending on the material with which the thermal actuator was made, when the hot arm temperature reaches its melting point then the actuator hot arm becomes much vulnerable to even small disturbance it undergoes and this may cause the bowing of thermal actuator hot arm. The bowing is a phenomenon where the hot arm structure becomes deformed due to quick cool off of the thermal actuator after actuation as a result of this hot arm deformation the thermal actuator behavior such as the displacement and force produced will be subjected to changes from their expected simulation value.

Thus it is better to operate the thermal actuator in the region where its hot arm temperature does not reach its melting point value corresponding to the material with which the thermal actuator was made up of hence the hot arm temperature profile obtained on simulation from ANSYS for thermal actuators made up titanium, stainless steel and brass helps to determine the working input current range of the thermal actuator so that it meets up to the needed requirements of displacement and force produced.

## 3.2 Simulation method

### *3.2.1 Modeling and Simulation in ANSYS*

The thermal actuator of the required dimension was modeled in ANSYS using blocks and the required material data was assigned to the created thermal actuator model according to the metal with which the thermal actuator was made up of. The simulation was carried out separately for the actuator made up of Titanium, Stainless steel and Brass. We varied the flexure arm length as a percentage of total length, which are 6% 7%, 8%, 10%, 20%, 30% and 40% by keeping the total actuator length constant. For each of the percentage mentioned above, the maximum hot arm temperature was noted by varying the current input to the actuator from 0.25 A to 1.25 A in steps of 0.25 A.

Applied boundary conditions in ANSYS for determining the temperature profile of the thermal actuator on actuation

1. The contact pads are anchored i.e. the degree of freedom was made zero in all three dimensions.
2. The contact pads temperatures are maintained at 30 degree Celsius.
3. The required voltage was applied across the contact pads to actuate the thermal actuator.

The temperature profile of the thermal actuator was determined to find the maximum hot arm temperature of the actuator on actuation, the figure 3.1 represents the temperature profile of the thermal actuator and the color scale at the bottom of the figure represents the temperature range the actuator had undergone on actuation in a VIBGYOR color pattern, the violet color represents the region of minimum temperature and in our case it represents the temperature assigned to the contact pads, the red color represents the region of maximum temperature and it is the temperature of the hot arm.

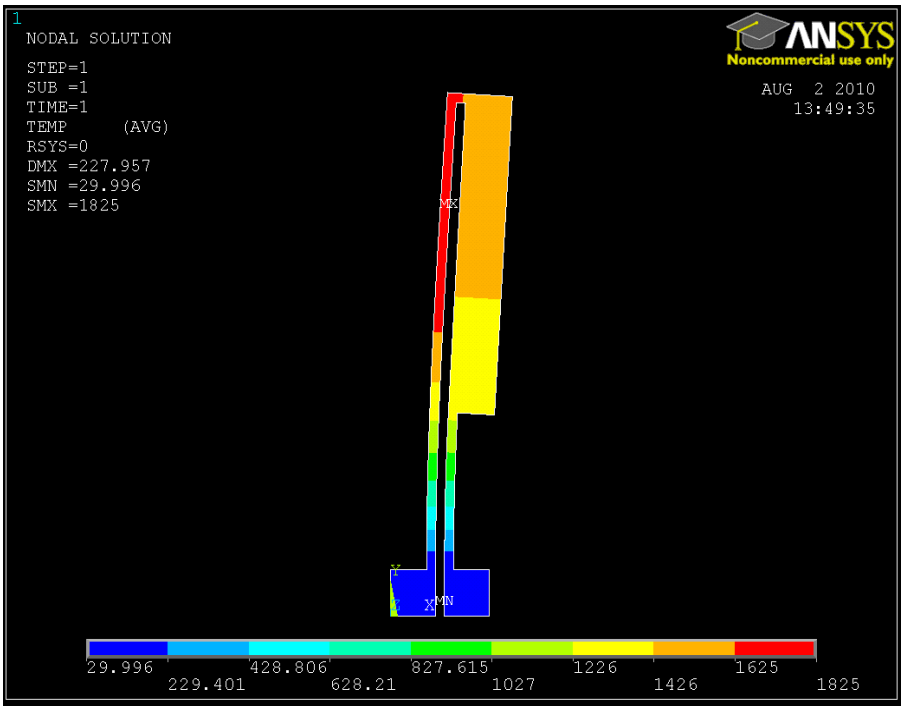


Figure 3.1 Temperature profile of the thermal actuator.

*3.2.2 Simulation Results*

The simulation was carried on for the three types of metal thermal actuators for their 6%, 7%, 8%, 10%, 20%, 30% and 40% profile by varying the actuation current from 0 to 1.25 A in steps of 0.25 A. The figure 3.2, 3.3 and 3.4 represents the maximum hot arm temperature of titanium, stainless steel and brass thermal actuators respectively.

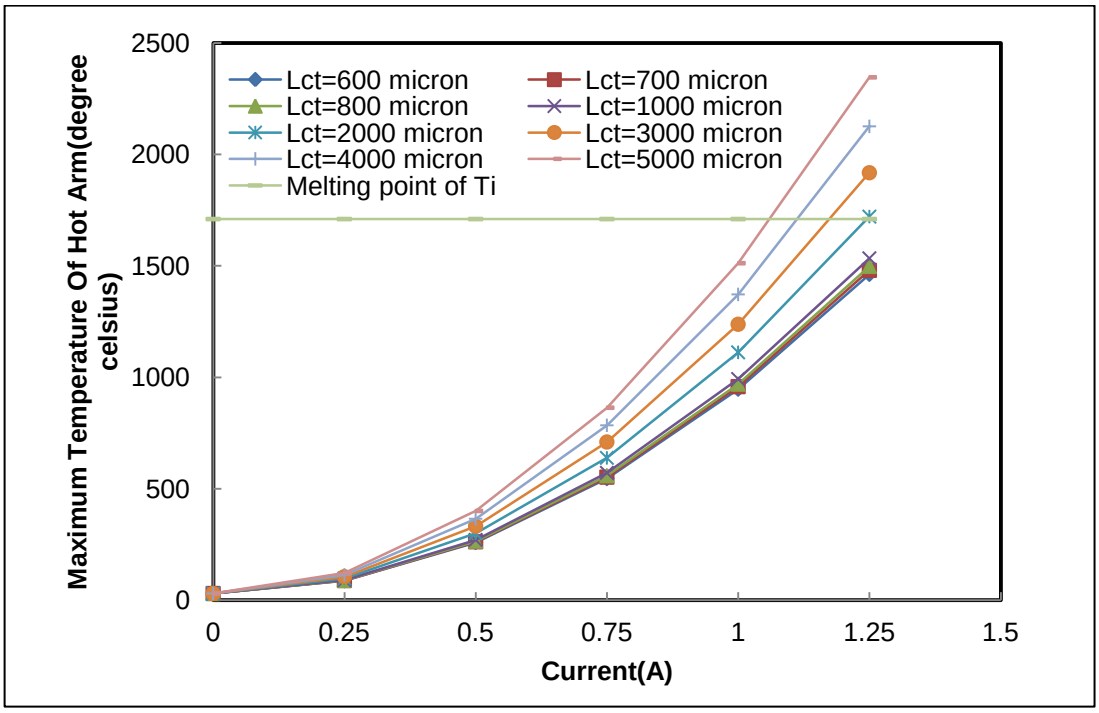


Figure 3.2 Maximum hot arm temperature for titanium thermal actuator.

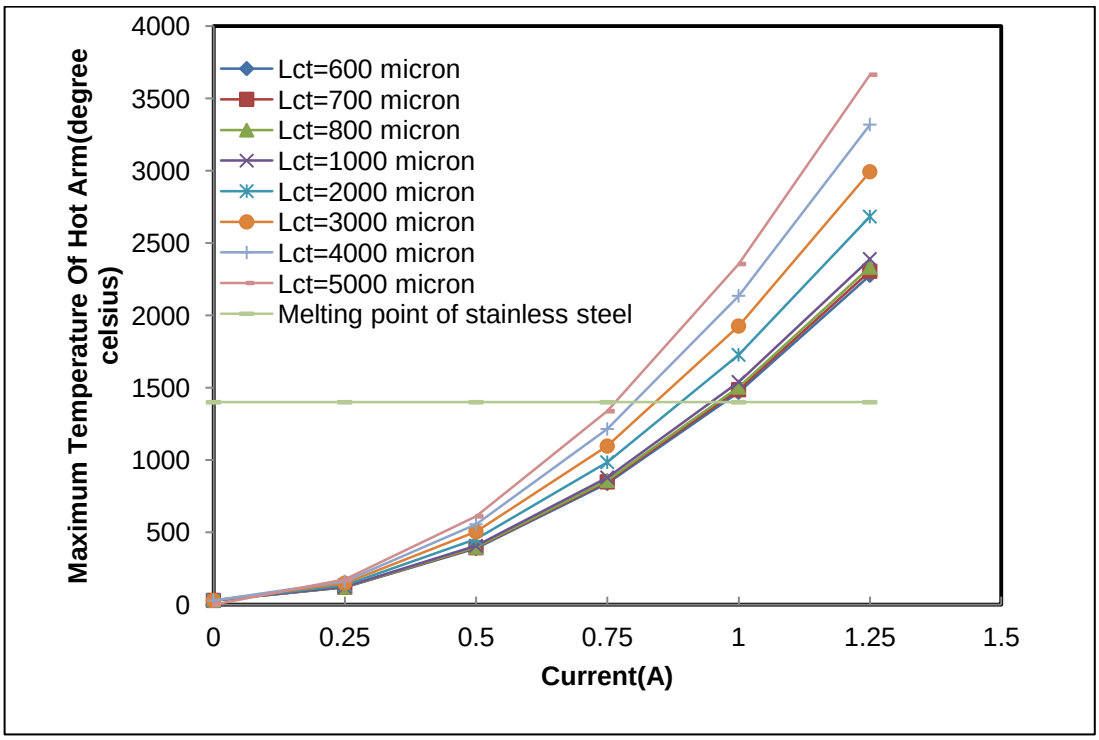


Figure 3.3 Maximum hot arm temperature for stainless steel thermal actuator.

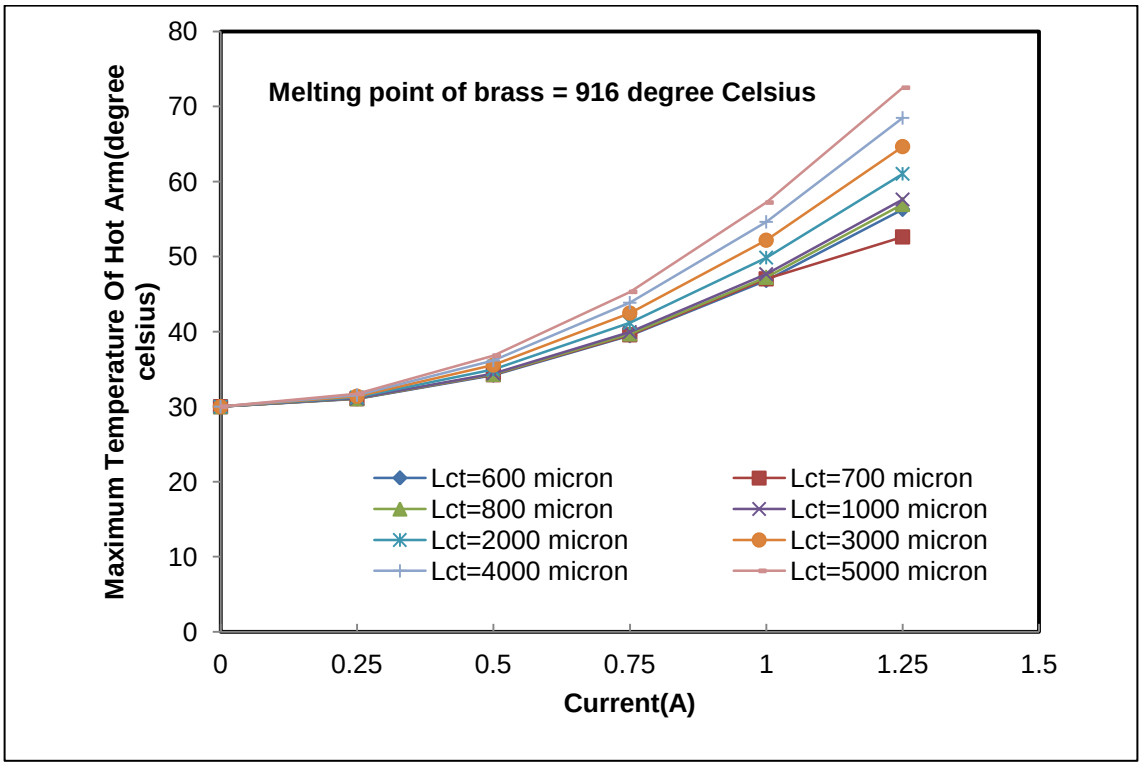


Figure 3.4 Maximum hot arm temperature for brass thermal actuator.

*3.2.3 Conclusion*

For an actuator input current range of 0.25 A to 1.25 A it can be observed from figure 3.2, 3.3 and 3.4 that the working input current range, the range within which the hot arm temperature does not reach its melting point for the 6% all the way through 40% thermal actuators was found to be more for Titanium thermal actuators compared to Stainless steel thermal actuators, the Brass thermal actuators hot arm temperature does not reach its melting point for a given current range of 0.25 A to 1.25 A.

# CHAPTER 4

# FORCE MEASUREMENT OF THERMAL ACTUATOR

## 4.1 Introduction

The force produced by thermal actuators was considered to be one of the important characteristics to determine the performance of the thermal actuator. Thermal actuator are known to produce much higher force on consuming less input power compared with other types of MEMS actuators [4] and it is because of this characteristics the thermal actuator has been used in wide applications involving lifting up of scanning mirror structure, moving shutters etc. [9]. In our case, the expected force value was much higher since the thermal actuator was made up of metals further this also helps in extending the application of thermal actuator needing high force requirements.

We determined the force produced by the thermal actuator under unloaded and loaded condition. In unloaded condition, the force required by the actuator to the produce the required displacement was determined on simulation using ANSYS and the force value thus obtained corresponds to the force that will be exerted by the thermal actuator at that value of displacement. In loaded condition, the force exerted by the actuator tip was determined using cantilever method of force determination.

## 4.2 Force Produced by Thermal Actuator under Unloaded Condition

### *4.2.1 Modeling and Simulation in ANSYS*

To determine this force, the thermal actuator was modeled and depending upon the metal with which the thermal actuator was made up of corresponding material property of the metal used was assigned to the modeled structure through meshing. The following boundary condition was then assigned

1. The contact pads are anchored i.e. the degree of freedom was made zero in all three dimensions.
2. A nodal force was applied to the top left most tip of the hot arm in the direction of motion of thermal actuator as shown in figure 4.1. In terms of ANSYS, a nodal force along X-direction was applied.

Simulation was then carried on by assigning a random value to the nodal force and then simulating the actuator so as to get the actuator's tip displacement value. The maximum displacement along X-direction produced by the actuator as a result of the applied force was determined followed by which the nodal force value was varied using trial and error method till the needed actuator tip displacement was achieved. The final nodal force value thus represents the force that will be exerted by the actuator at that particular value of displacement. We determined the force value corresponding to the actuator tip displacement achieved previously during the displacement measurement for 6%, 7%, 8%, 10%, 20%, 30% and 40% thermal actuators each made up metals like titanium, stainless steel and brass.

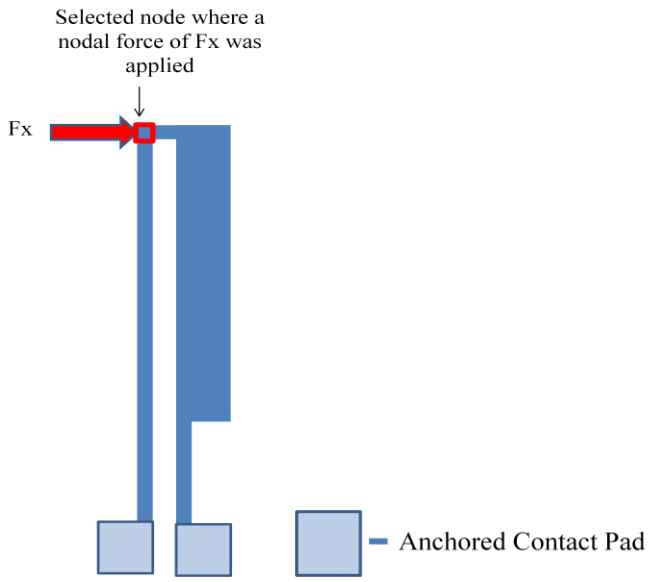


Figure 4.1 Applied nodal force on simulation to determine the force produced by actuator under unloaded condition.

*4.2.2 Simulation Results*

To make the plot of the force exerted by the thermal actuator under unloaded condition quite simpler, the nodal force value obtained on simulation was plotted against the actuator input current instead of displacement since the displacement values corresponding to the actuator input current values are known from the previously obtained plot as shown in figure 2.2, 2.4 and 2.6 for Titanium, Stainless steel and Brass thermal actuators. The figure 4.2, 4.3 and 4.4 shown below describes the force produced by the Titanium, Stainless steel and Brass thermal actuators tip under unloaded condition.

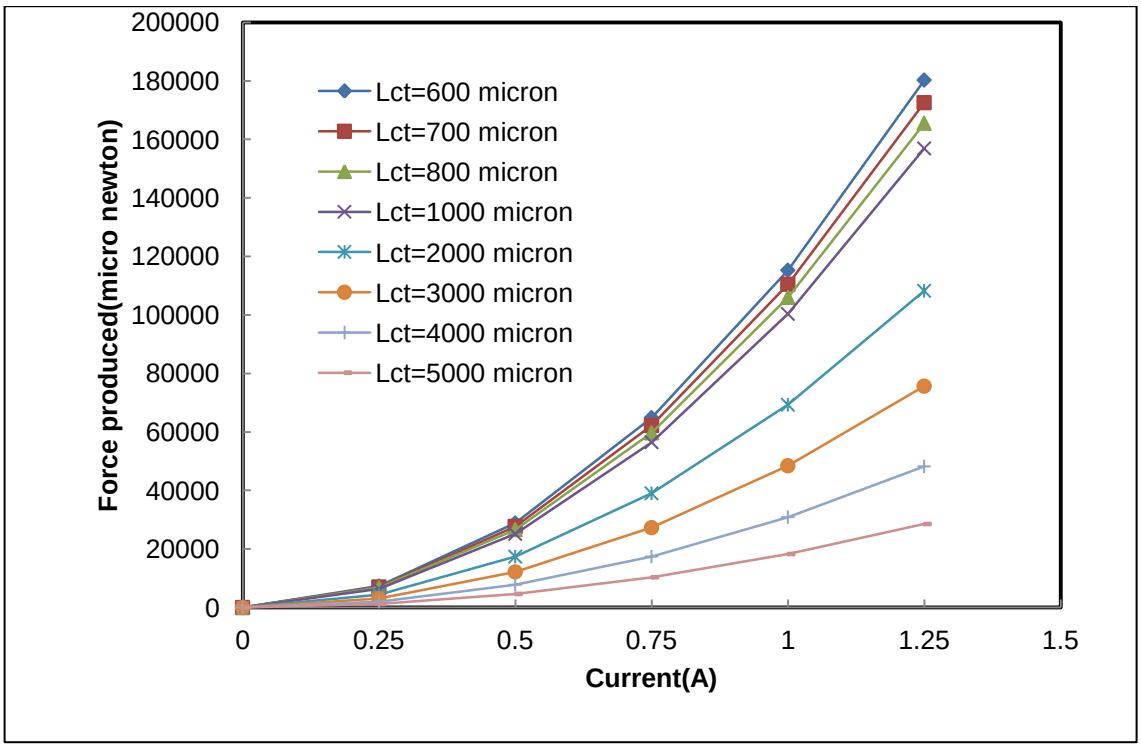


Figure 4.2 Force produced by Titanium thermal actuators tip under unloaded condition.

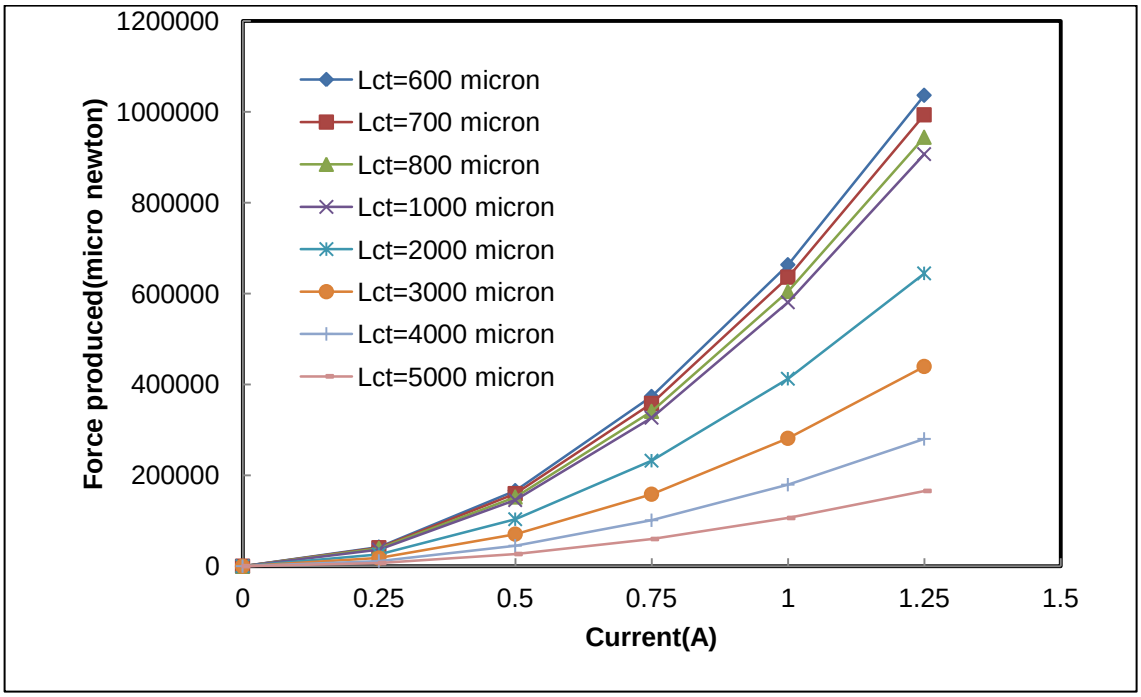


Figure 4.3 Force produced by Stainless steel thermal actuators tip under unloaded condition.

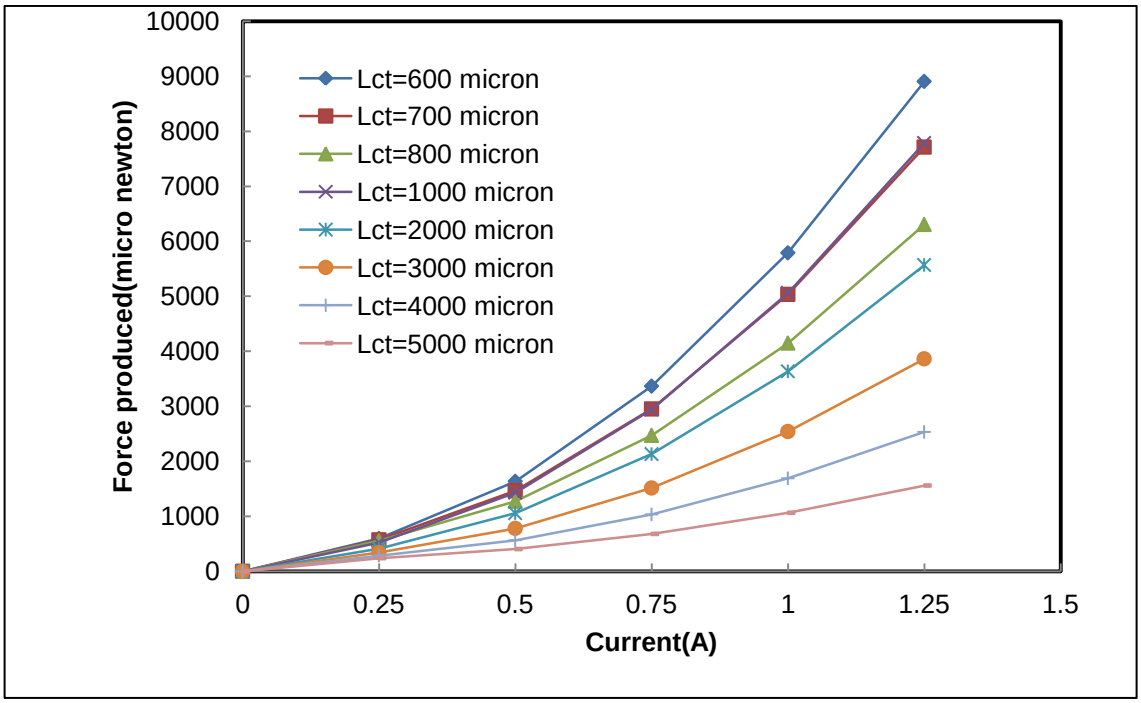


Figure 4.4 Force produced by Brass thermal actuators tip under unloaded condition.

The table 4.1, 4.2 and 4.3 listed below represents 7% Titanium, stainless steel and brass thermal actuator, its displacement corresponding to the actuator input current value and the force exerted at that particular displacement value and also the spring constant of the 7% thermal actuator obtained by dividing the tabulated force value with the displacement value for each value of the actuator input current value. Small discrepancies can be observed in the spring constant value mainly due to the trial and error approach to determine the force value.

Table 4.1 Spring constant of a 7% Titanium thermal actuator

| Current (Ampere) | Displacement (micrometer) | Force (micro newton) | Spring constant (micro newton / micrometer) |
|---|---|---|---|
| 0.25 | 19.983 | 7013 | 350.9483061 |
| 0.5 | 79.166 | 27717.29 | 350.1160852 |
| 0.75 | 177.804 | 62208.5 | 349.8712065 |
| 1 | 315.898 | 110510.5 | 349.8296919 |
| 1.25 | 493.446 | 172605.9 | 349.7969383 |

Table 4.2 Spring constant of a 7% Stainless steel thermal actuator

| Current (Ampere) | Displacement (micrometer) | Force (micro newton) | Spring constant (micro meterewton/ micrometer) |
|---|---|---|---|
| 0.25 | 61.761 | 40643 | 658.069008 |
| 0.5 | 245.526 | 159735.5 | 650.5848668 |
| 0.75 | 551.801 | 358224.2 | 649.1909221 |
| 1 | 980.586 | 636105.5 | 648.6993492 |
| 1.25 | 1532 | 993382.9 | 648.4222585 |

Table 4.3 Spring constant of a 7% Brass thermal actuator

| Current (Ampere) | Displacement (micrometer) | Force (micro newton) | Spring constant (micro meterewton/ micrometer) |
|---|---|---|---|
| 0.25 | 1.437 | 572 | 398.0514962 |
| 0.5 | 3.964 | 1463.932 | 369.3067608 |
| 0.75 | 8.175 | 2951.409 | 361.0286239 |
| 1 | 14.071 | 5034.431 | 357.7877194 |
| 1.25 | 21.652 | 7712.582 | 356.2064474 |

To compare the force produced by titanium, stainless steel and brass thermal actuators under unloaded condition, The force exerted at 100 micro meter displacement by 6%, 7%, 8%, 10%, 20%, 30% and 40% thermal actuators made up the above mentioned three metals and also the power consumed by the above thermal actuators to produce an actuator tip displacement of 100 micro meter was also determined on simulation. It can be observed from the from figure 4.5 that the force exerted at 100 micro meter displacement was found to be more for stainless steel thermal actuators on comparison with brass and titanium thermal actuators and to our surprise we found brass thermal actuators to exert more force in comparison with titanium thermal actuators but these results alone cannot be used as an parameter to conclude that brass thermal actuators are better than titanium thermal actuators for the brass thermal actuator consumes much more input power to exert such forces when compared to titanium thermal actuators. The figure 4.6 represents the power consumed by the 7% titanium, stainless steel and brass thermal actuators to produce an actuator tip displacement of 100 micro meters.

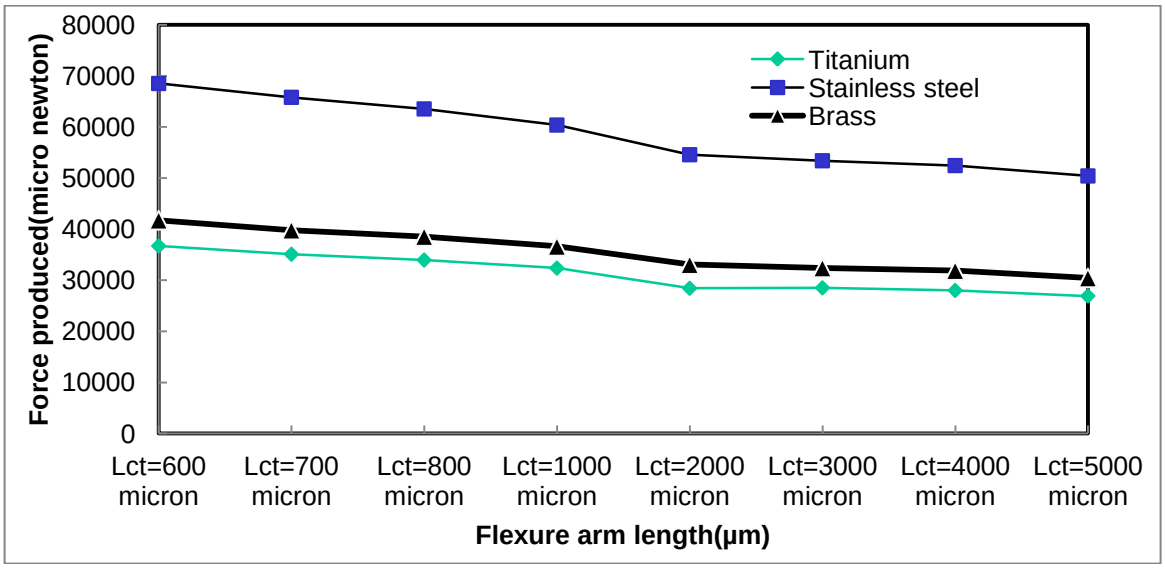


Figure 4.5 Force produced by thermal actuators tip under unloaded condition to produce an actuator tip displacement of 100 micro meter.

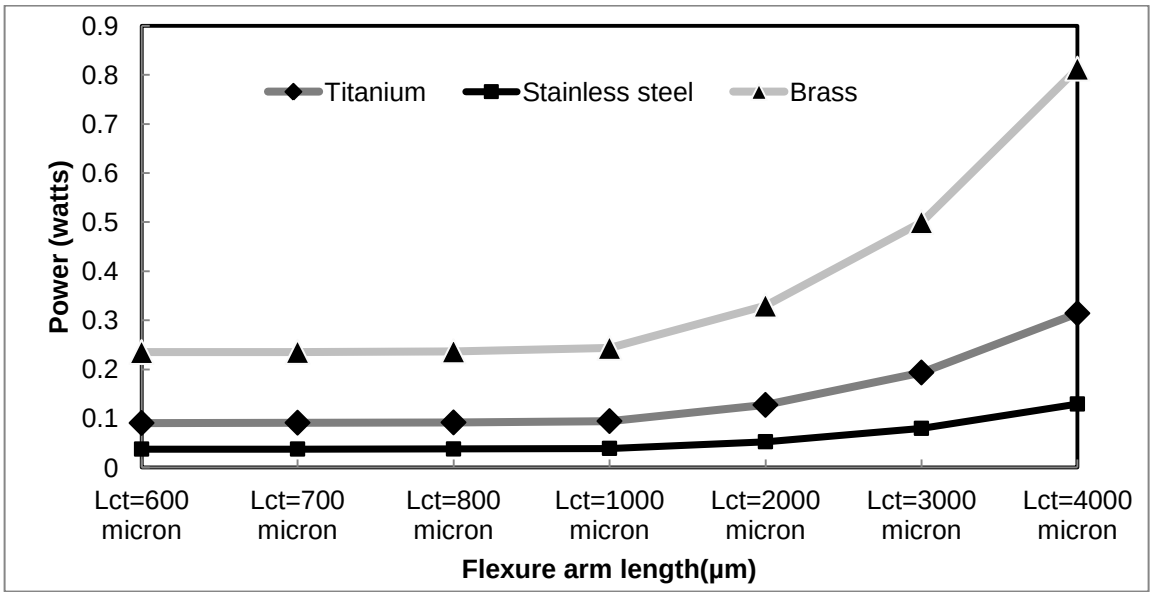


Figure 4.6 Power consumed by thermal actuators under unloaded condition to produce an tip displacement of 100 micro meter.

## 4.3 Force Produced by Thermal Actuator under loaded Condition

### *4.3.1 Modeling and Simulation in ANSYS*

In this case the thermal actuator was loaded initially and the force exerted by the actuator on the load was determined both through simulation and also through experiment. We used the cantilever method to determine the force exerted by the actuator tip on the cantilever [5]. In the cantilever method of force determination, a straight beam cantilever was used with its base end anchored to the substrate; an unknown force was then applied to it at a known distance from the anchored end of the cantilever and depending upon the tip displacement of the cantilever, the unknown force can be determined. Larger the magnitude of cantilever tip displacement means larger the magnitude of force [3].

To determine this force, the thermal actuator along with the cantilever was modeled as shown in figure 4.7 and depending upon the metal with which the thermal actuator was made up of corresponding material property of the metal used was assigned to the modeled structure including the cantilever through meshing. The following boundary condition was then assigned

1. The contact pads are anchored i.e. the degree of freedom was made zero in all three dimensions.
2. The metal strip connecting the thermal actuator with the cantilever was restricted to move only in horizontal X- direction.
3. Cantilever was anchored at one of its end and its anchored end was maintained at 30 degree Celsius.
4. The contact pads temperatures of the thermal actuator was maintained at 30 degree Celsius.
5. The required voltage was then applied across the contact pads to actuate the thermal actuator.

Simulation was then carried on by assigning suitable voltage value across the thermal actuator contact pads that produced the required current values for actuation. The displacement of the cantilever along X-direction at the point of contact between the thermal actuator tip with the cantilever along the cantilever's length was noted down. The applied force by the actuator tip on the cantilever was then determined using a suitable formula. We determined the force produced by the thermal actuator under loaded conditions for 6%, 7%, 8%, 10%, 20%, 30% and 40% thermal actuators each made up metals like titanium, stainless steel and brass using the cantilever method of force determination.

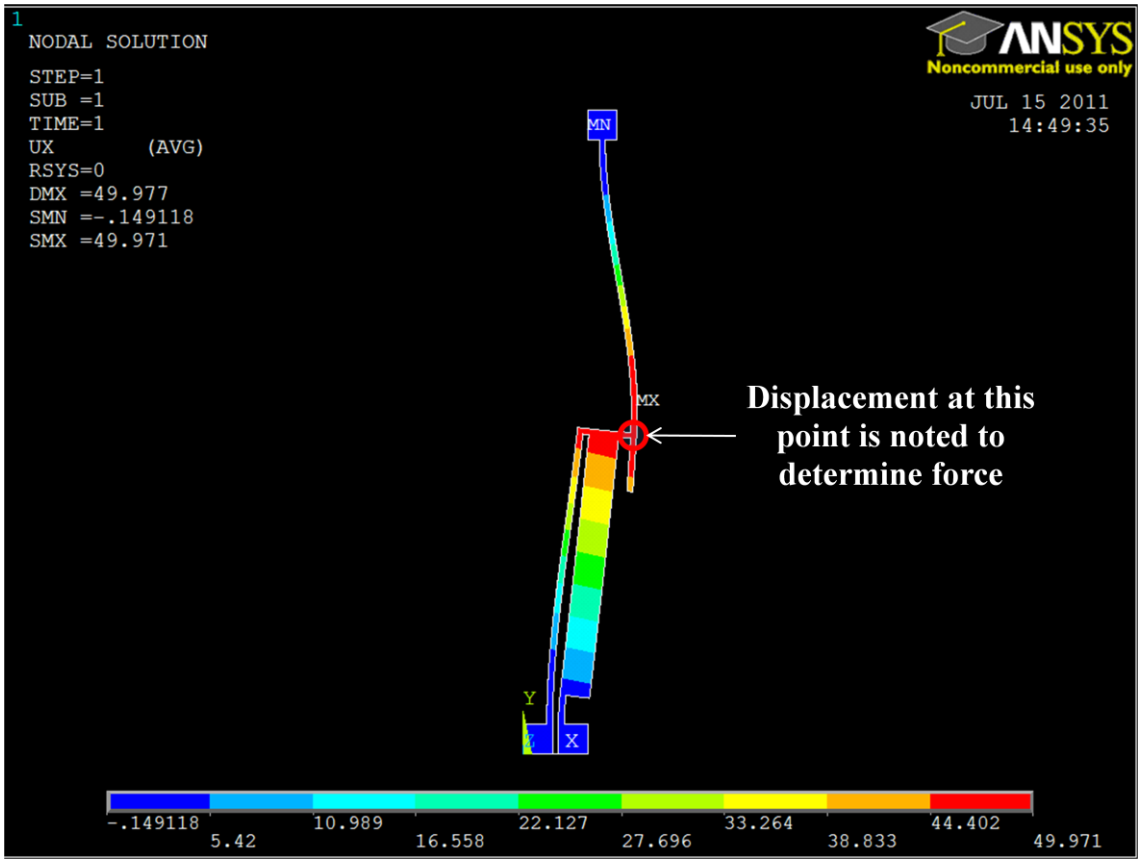


Figure 4.7 ANSYS simulation to determine the force produced by thermal actuator using cantilever method under loaded condition.

*4.3.2 Simulation results*

We can observe from figure 4.8, 4.9 and 4.10 that for thermal actuators made up of titanium and stainless steel, the force exerted by the thermal actuator tip on the cantilever increases as we go from 6%, 7% and all the way through 30% but starts to decrease on 40%, the reason could be due to the fact that the hot arm temperature increases as we go from 6% all the way through 40% thermal actuators and in case of titanium and stainless steel at 40%, the temperature of hot arm would have reached a point where it begins to melt thus the force exerted by it on the cantilever was found to be reduced. In case of brass, we can observe that the force keeps on decreasing as we go from 6% all the way through 40% for actuation current ranging from 0A to 0.75A since the increase in flexure arm length results in decrease in the force output of the thermal actuator on the cantilever and also for brass the hot arm temperature increase was observed to be very low as we go from 6% all the way through 40% at a particular value of actuation current thus the force produced by the hot arm which results in the horizontal motion of actuator tip will not increase much so as we keep increasing the flexure arm length it may reduce the force action on the cantilever by impeding the force exerted due to the hot arm. At current range from 1A to 1.25 A the force produced by the actuator increases as we go from 6 to 20% but decreases as we move on to 30% and 40% this could be because the hot arm temperature increase was now sufficient enough to exceed the impeding force exerted by the flexure arm but again at 30% and 40%, force due to the expanding flexure arm increases hence the force output decreases.

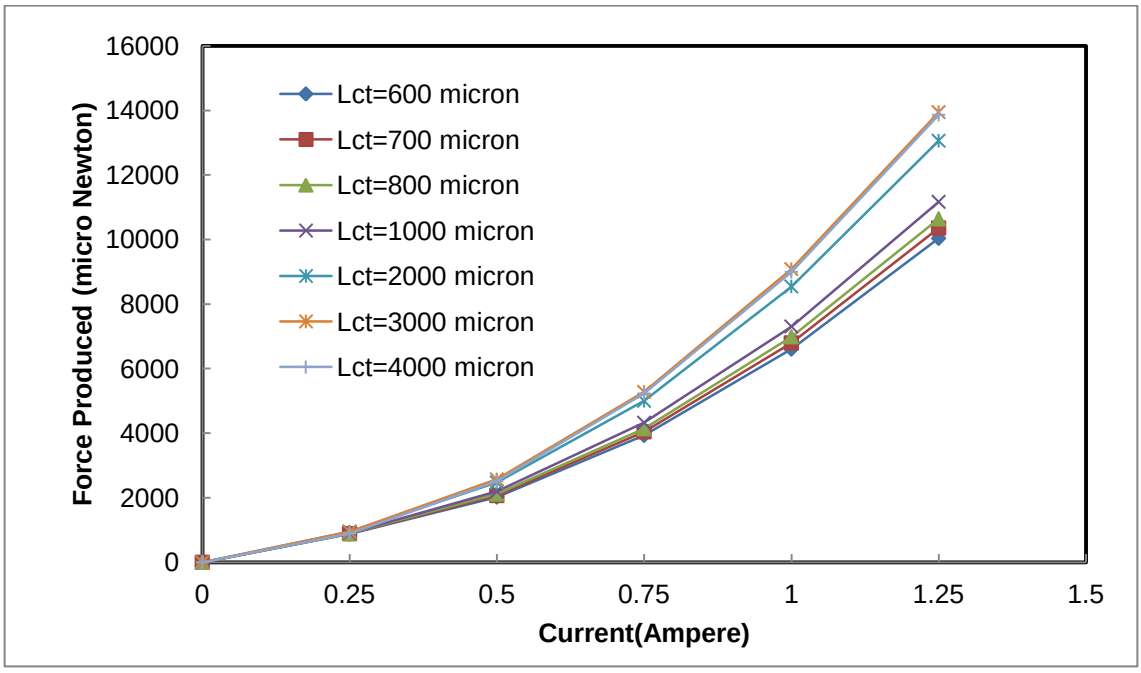


Figure 4.8 Force produced by Titanium thermal actuators tip under loaded condition.

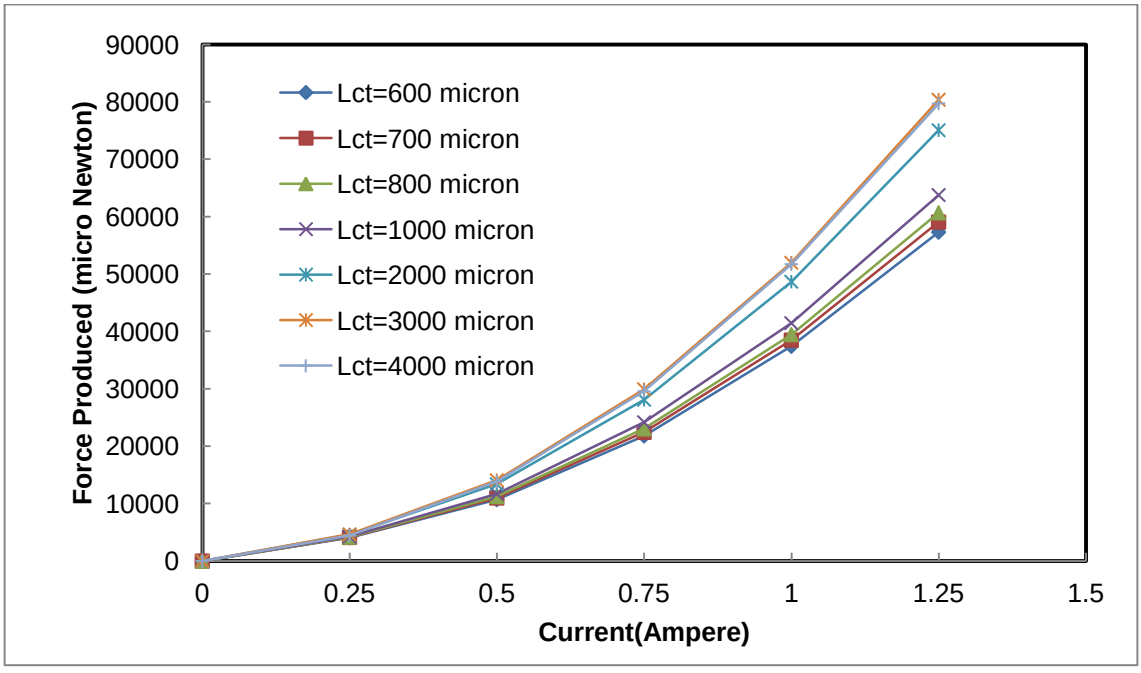


Figure 4.9 Force produced by Stainless steel thermal actuators tip under loaded condition.

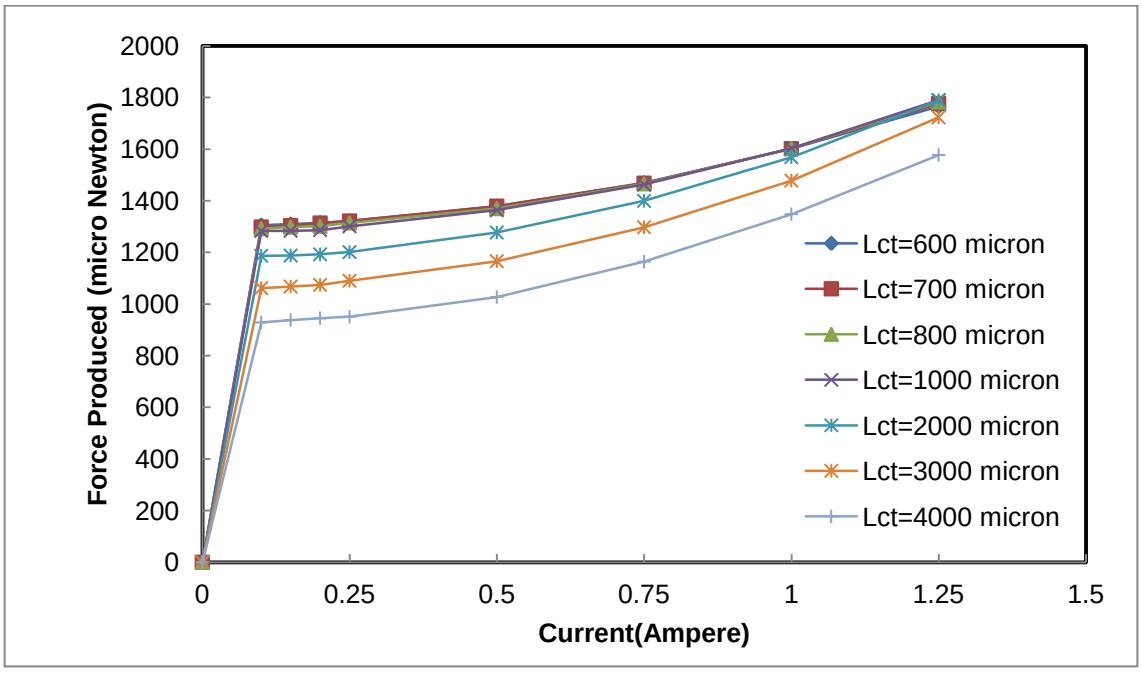


Figure 4.10 Force produced by Brass thermal actuators tip under loaded condition.

*4.3.3 Experimental setup*

The experimental setup for determining the force produced by the thermal actuator was same as it was for measuring actuator tip displacement but the only difference was that a cantilever was now introduced so as to determine the force produced by the actuator tip under loaded condition. Further some modification was made to the thermal actuator tip so as to make it engage with the cantilever during actuation. The dimensions of the cantilever used for force measurement and the dimensions of the protruding actuator tip are as shown in figure 4.11. The semi arc part was made on the cantilever so as to make the protruding tip of the thermal actuator engage with the cantilever and also to restrict the force exerted by the thermal actuator tip along the horizontal or x-direction.

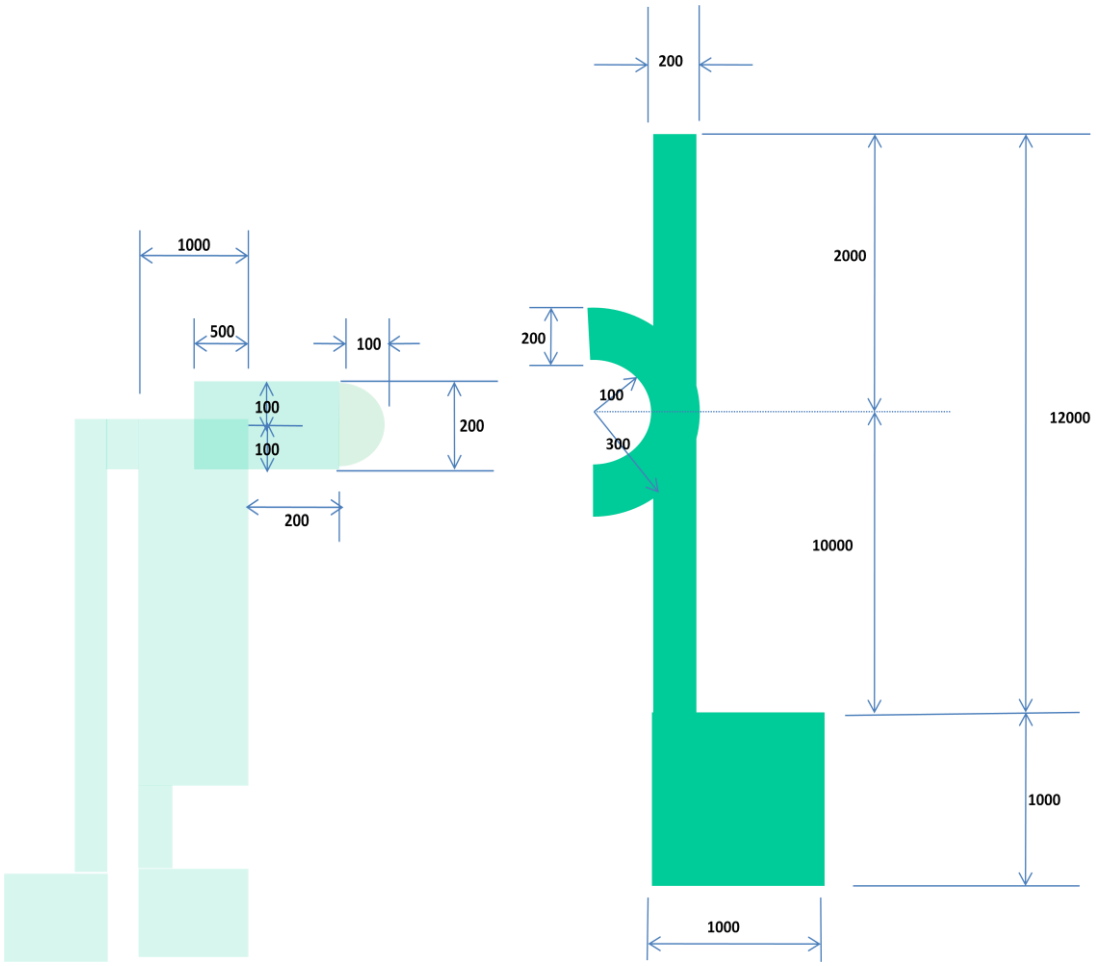


All dimensions are in micro meters

Figure 4.11 Dimension of thermal actuator protruding tip and cantilever used for force measurement.

The figure 4.12 represents the metal thermal actuator and arrangement of thermal actuator along with the cantilever for force measurement. The cantilever was kept upside down so as to ease the process of aligning its arc portion with the protruding thermal actuator tip for measuring force. We used the same metal type of thermal actuator and cantilever while measuring force, for titanium actuator force measurement titanium cantilever was used and for brass thermal actuator force measurement brass cantilever was used.

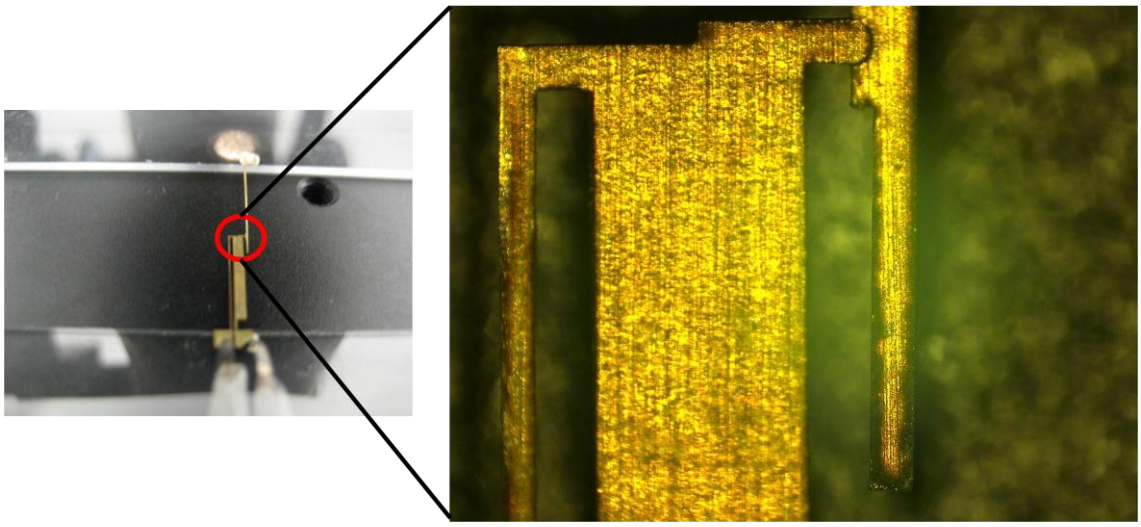

Figure 4.12 Thermal actuator and cantilever experimental setup for force measurement with the magnified portion of the circled region on the left to its right.

*4.3.4 Experimental Results*

The cantilever displacement was measured for 6%, 7%, 8%, 10%, 20%, 30% and 40% thermal actuators made up of metals like titanium, stainless steel and brass by exciting each of them with current ranging from 0.25 A to 1.25 A in steps of 0.25 A. The experimentally obtained displacement value was then plotted against the cantilever displacement value obtained through simulation in ANSYS so as to validate the experimental data with the simulation data.

We can observe from figure 4.13 and 4.15 that for titanium that simulation data falls slightly below the experimental data as we go from 6% all the way 40%, the reason behind this was because the thermal actuator and the cantilever were not exactly lying in the same level plane so not all force produced by the thermal actuator was delivered to the cantilever hence we can observe a small deviation between the simulated and experimental data.

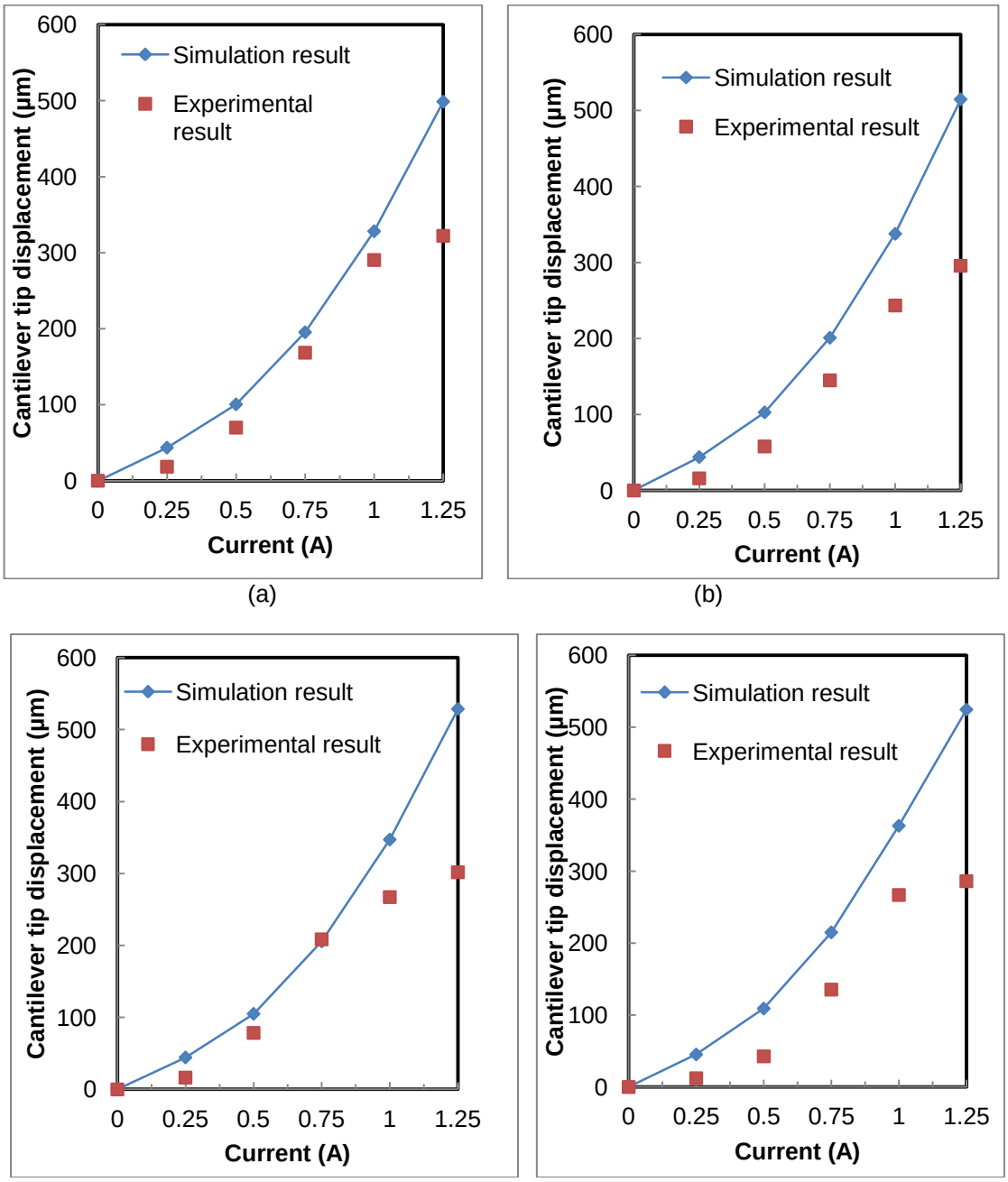


Figure 4.13 Cantilever displacement produced by titanium thermal actuator during force measurement (a) 6% (b) 7% (c) 8% (d) 10%.

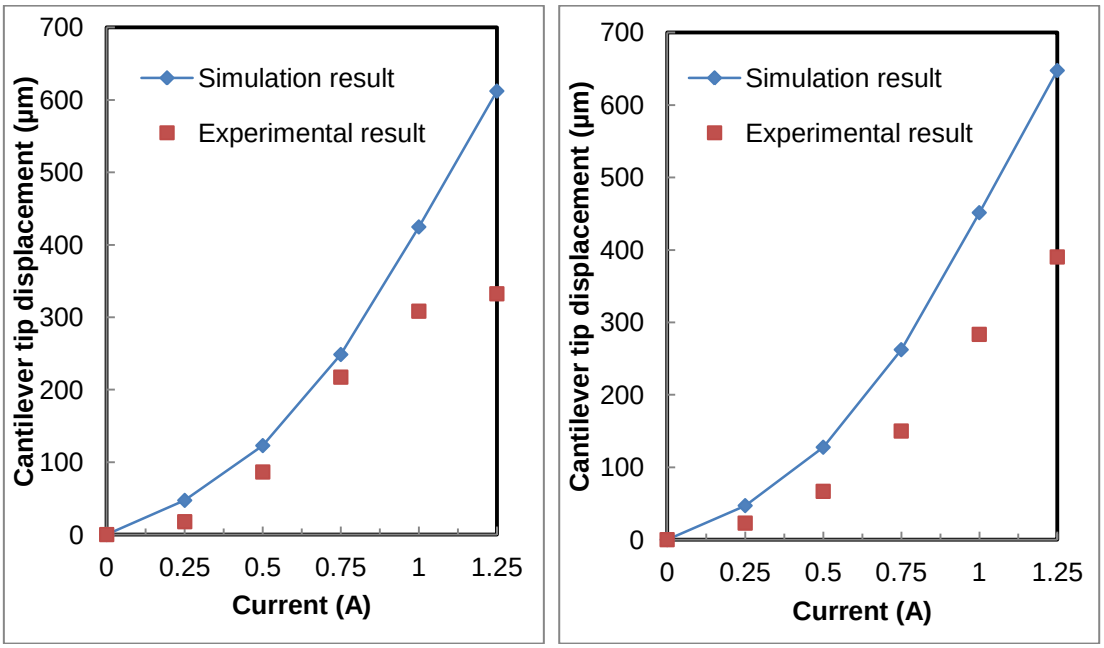


(a) (b)

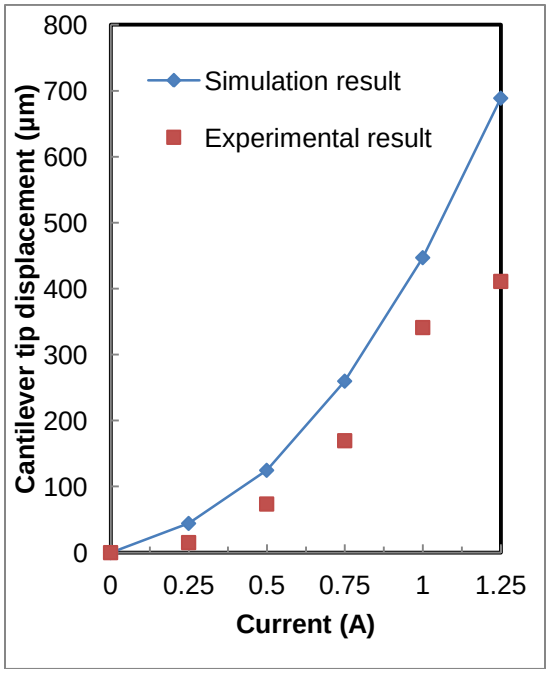


(c)

Figure 4.14 Cantilever displacement produced by titanium thermal actuator during force measurement (a) 20% (b) 30% and (c) 40%.

We can observe from figure 4.15 and 4.16 that for stainless steel the simulation data falls below the experimental data as we go from 6% all the way through 40%, the reason behind this was because the thermal actuator and the cantilever were not exactly lying in the same plane so not all force produced by the thermal actuator was delivered to the cantilever hence we can observe a small deviation between the simulated and experimental data. As we can observe from 6% all way through 40% at a current value of 0.25 A, the experiment cantilever displacement and the simulation cantilever displacement value differ not much but as the current increases beyond it the difference becomes much more amplified. Since the hot arm temperature of stainless becomes very much higher as we increase the current, which results in the enormous increase in cantilever displacement magnitude for each step in current value hence under such circumstances even a slight deformity in thermal actuator shape and dimension can result in affecting the thermal actuator behavior. The thermal actuator will displace vertically more comparatively with respect to the horizontal displacement hence the area of contact between the thermal actuator tip and the contact decreases thus the resulting cantilever displacement were also found to be marginally lesser than the expected simulation value.

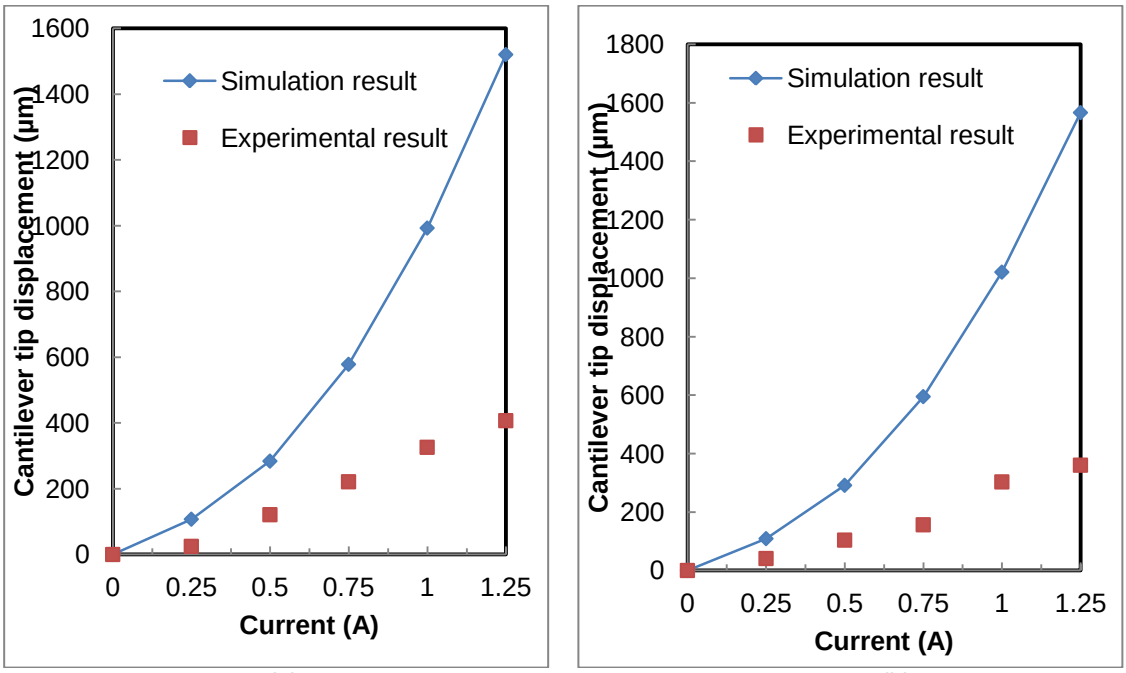


(a)




(b)

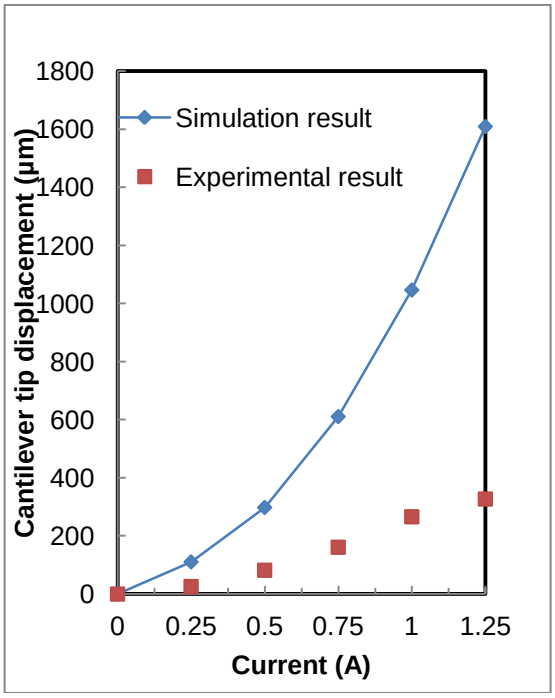


(c)

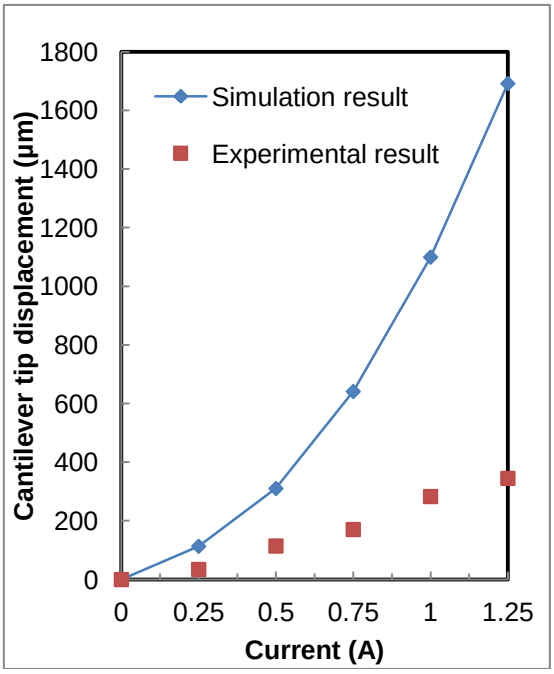


(d)

Figure 4.15 Cantilever displacement produced by stainless steel thermal actuator during force measurement (a) 6% (b) 7% (c) 8% (d) 10%.

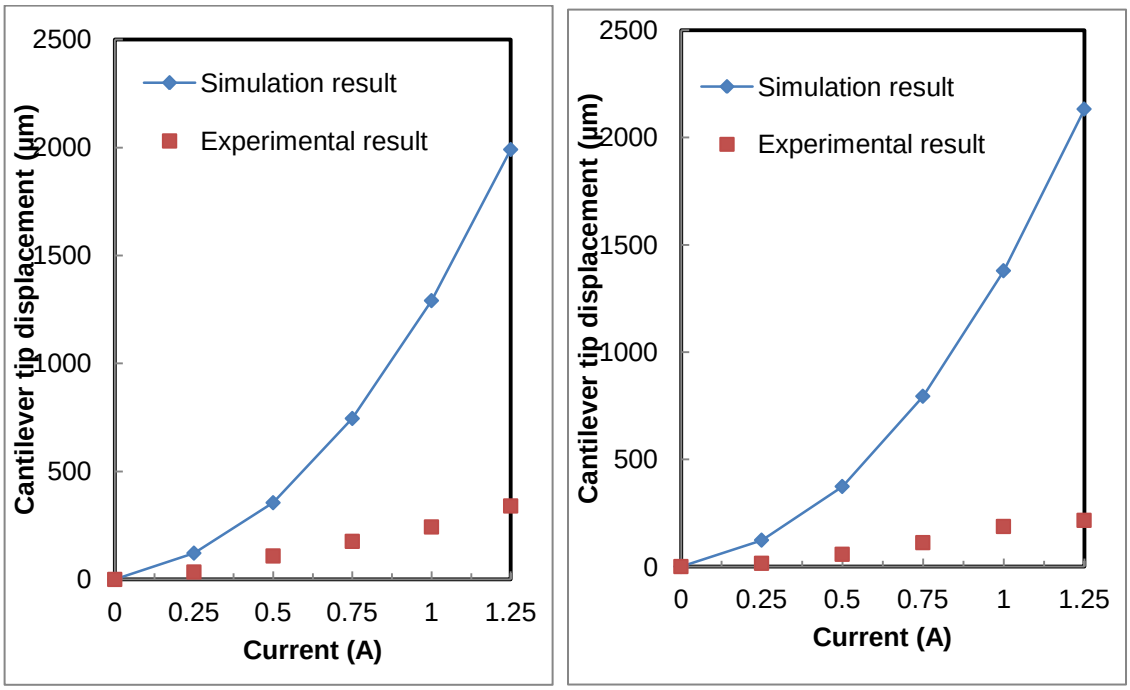


(a) (b)

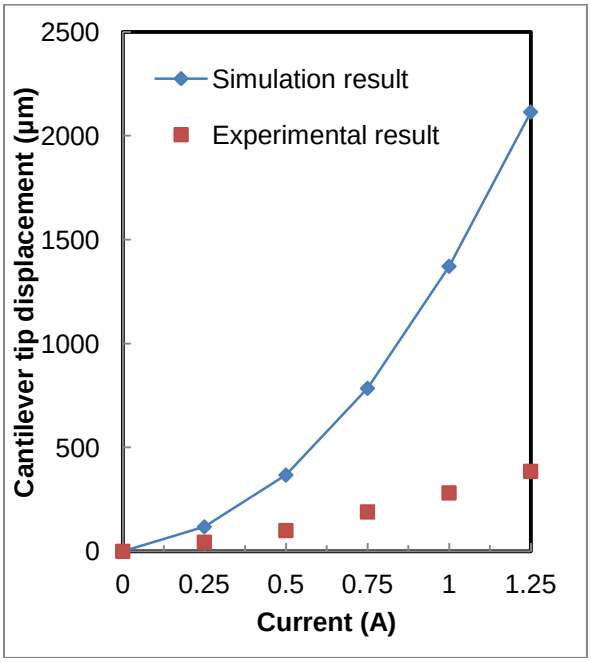


(c)

Figure 4.16 Cantilever displacement produced by stainless steel thermal actuator during force measurement (a) 20% (b) 30% and (c) 40%.

We can observe from figure 4.17, 4.18 and 4.19 that for brass, the cantilever displacement value obtained from experiment becomes much higher than the simulation data as we go from 6% all way through to 40%. The reason is due to the reduced hot arm width of the thermal actuator obtained after laser micromachining and also due to the fact that assigned material properties for brass for simulation and the actual material properties of the brass metal from manufacturers may not be the exact and are subjected to variation, which may be the cause for the difference in cantilever displacement data as observed.

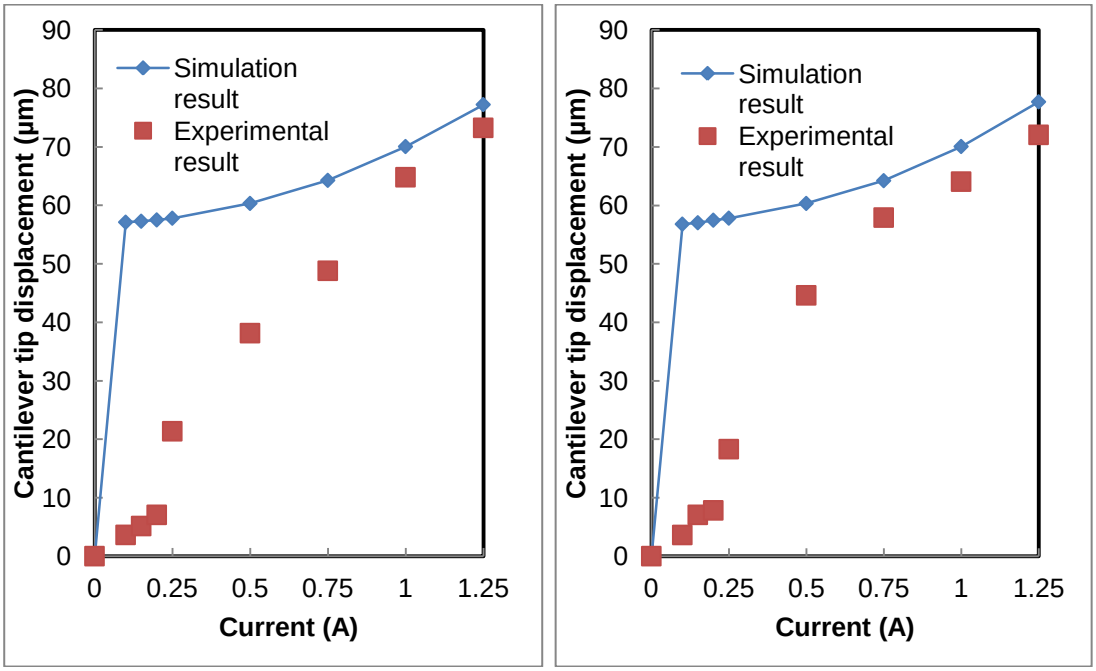


(a) (b)

Figure 4.17 Cantilever displacement produced by Brass thermal actuator during force measurement (a) 6% (b) 7%.

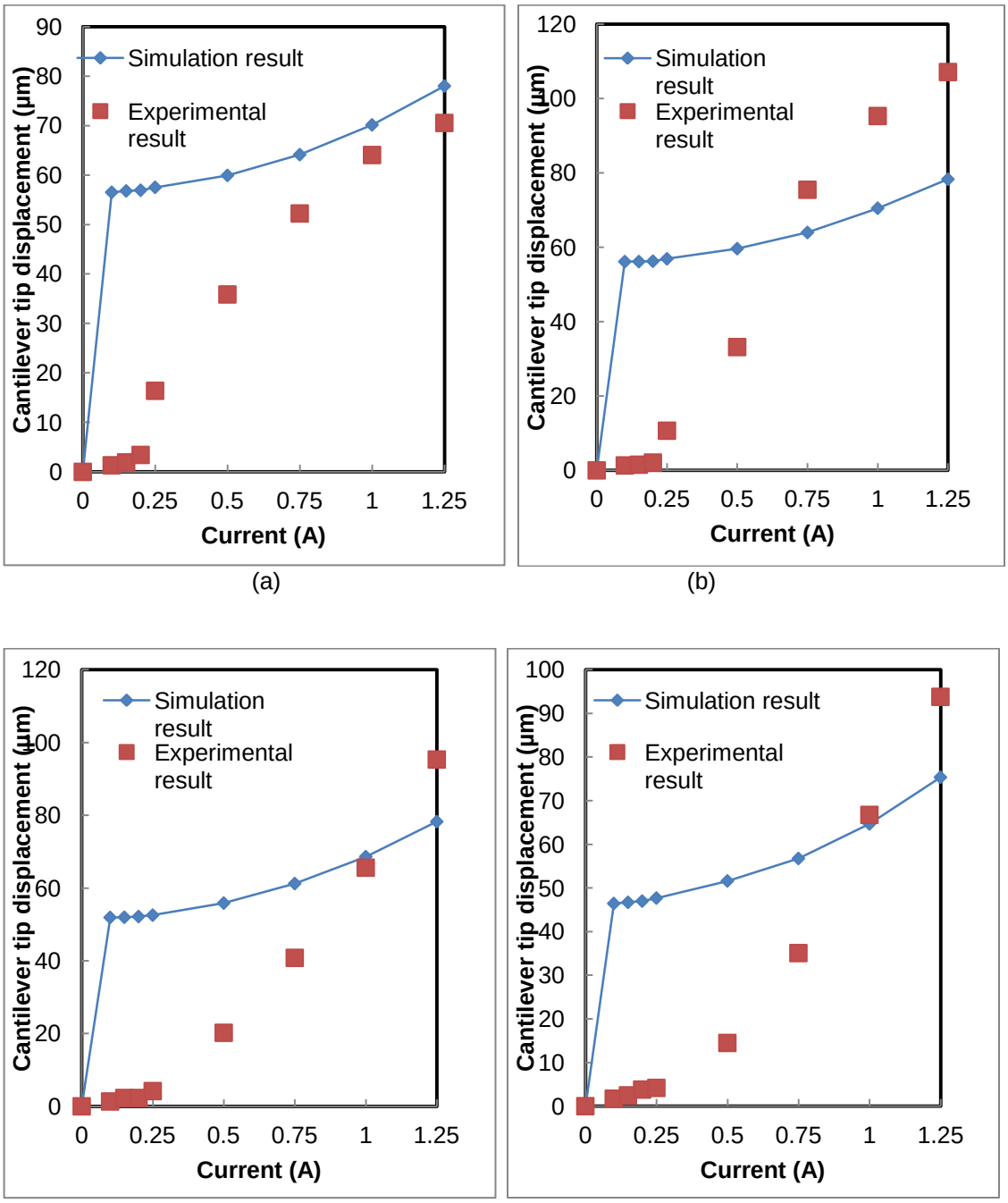


Figure 4.18 Cantilever displacement produced by Brass thermal actuator during force measurement (a) 8% (b) 10% (c) 20% (d) 30%.

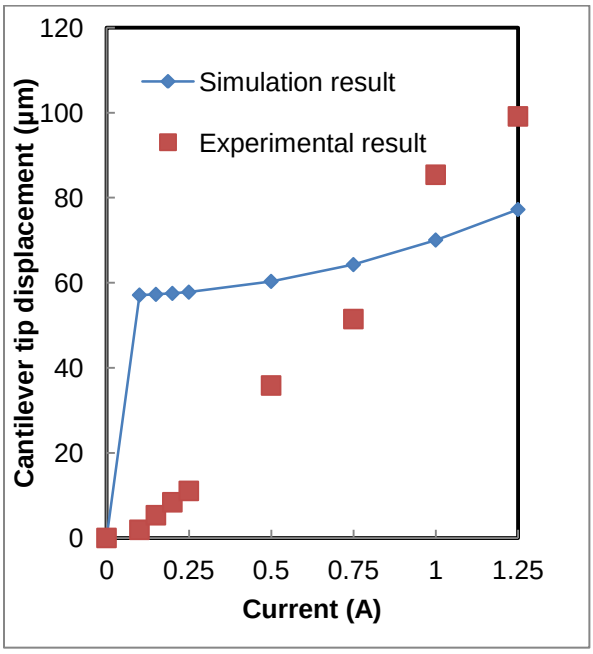


Figure 4.19 Cantilever displacement produced by 40% Brass thermal actuator during force measurement.

## 4.4 Conclusion

On the plot of the Current versus Cantilever displacement for 6% through 40% thermal actuators made up of titanium, stainless steel and brass, we can say that the stainless steel thermal actuator produces much more force compared to titanium and brass thermal actuator based on the cantilever displacement values.

# CHAPTER 5

# COMPARITIVE STUDY OF METAL THERMAL ACTUATORS

## 5.1 Introduction

To determine the best metal thermal actuator, we need to determine its behavior with respect to displacement, force produced, power consumed and also the working current range. Having determined the above behavior of thermal actuator we now can conclude the best of the three metal thermal actuators but their use depends upon the application so in this chapter we just classified titanium, stainless steel and brass based on their behaviors.

## 5.2 Conclusion

The conclusion are listed below in table 5.1 for all the three metal type thermal actuators are based on their working performance in the current range from 0 to 1.25 Ampere. The working current range describes the current range within which the maximum temperature of the hot arm does not reach its melting point onset value. We can observe from figure 5.1 that the stainless steel thermal actuator's hot arm starts reaching its melting point value at current value close to 1 ampere for 6% and the current value starts decreasing slowly as we go from 6% all way through 40%. In case of titanium the hot arm start reaches its melting point starting from 20% onwards at a current value of around 1.2 Ampere. The reason behind this was that the stainless steel has higher resistance compared to titanium hence its hot arm temperature also reaches its melting point quicker than titanium. Brass was not taken into consideration for its hot arm temperature never reached the melting point for the given input current range of 0 to 1.25 A for 6% all way through 40%. Also figure 5.2 describes the maximum displacement of the actuator tip when the thermal actuator hot arm temperature reaches its melting point.

Table 5.1 Comparative study of Titanium, Stainless steel and Brass thermal actuators

| | Titanium | Stainless steel | Brass |
|---|---|---|---|
| Displacement | Lesser than stainless steel but much more than brass | Best of the three | Much lesser than titanium and stainless steel |
| Force produced under loaded condition | Lesser than stainless steel but much more than brass | Best of the three | Lesser than stainless steel but more than titanium |
| Working current range | More than stainless steel and lesser than brass | Lesser than brass and titanium | Much more than titanium and stainless steel |
| Power consumed | Lesser than brass but more than stainless steel | Consumes less power of the three | More than stainless steel and titanium |

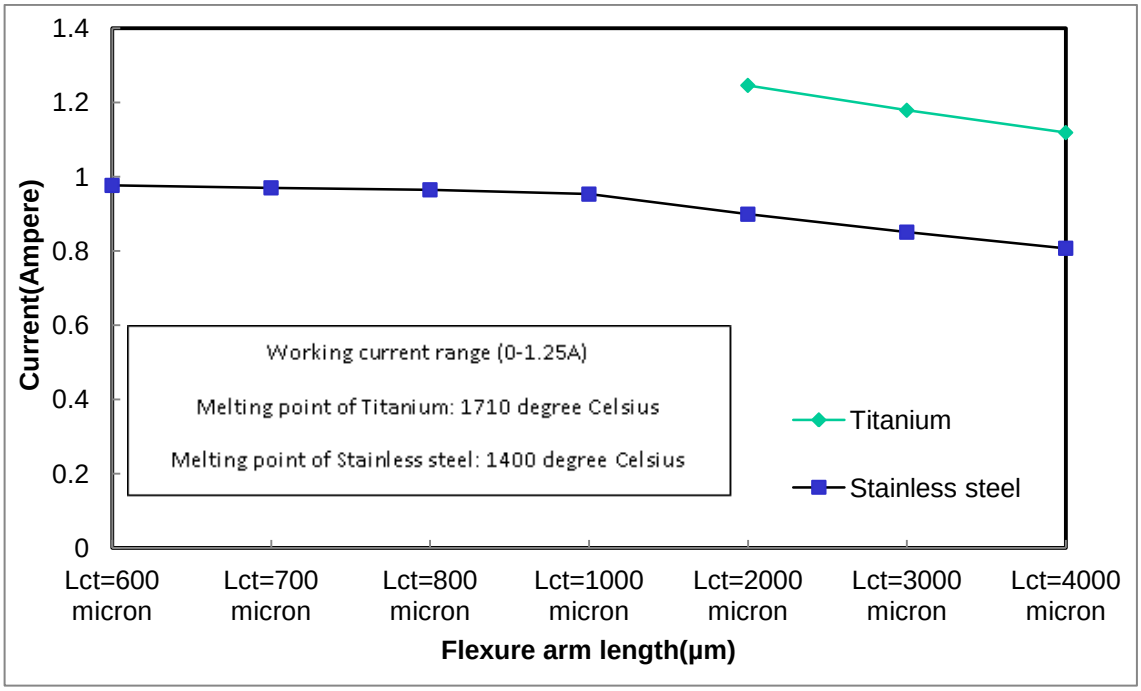


Figure 5.1 Current value at which the maximum hot arm temperature of the thermal actuator reaches the melting point.

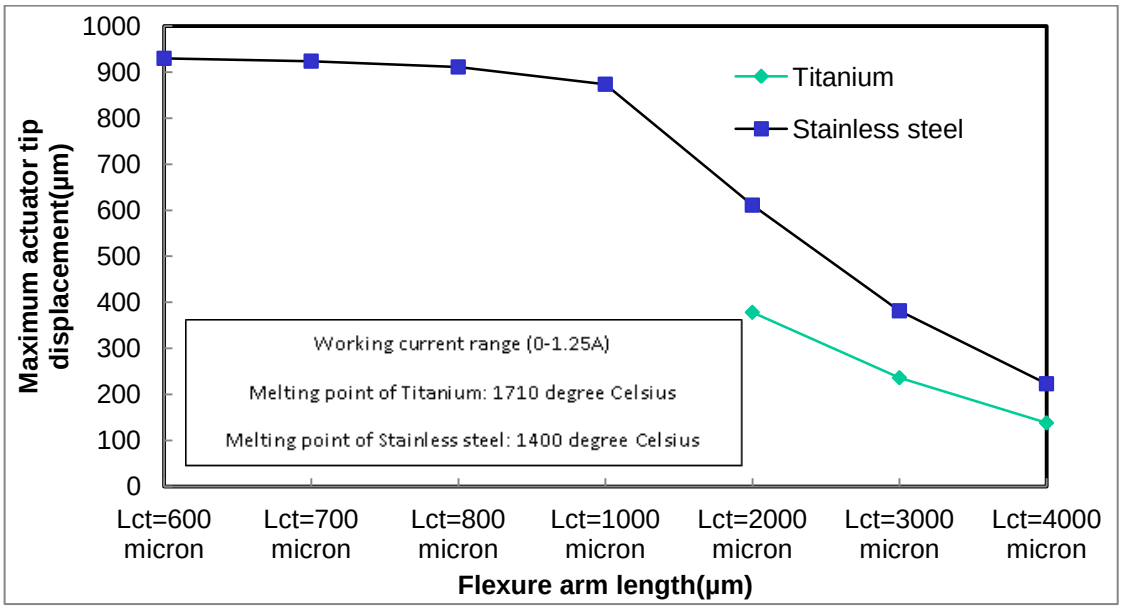


Figure 5.2 Maximum actuator tip displacement when the maximum hot arm temperature of the thermal actuator reaches the melting point.

## 5.3 Resonant Frequency

The Resonant frequency of the three metal thermal actuators was determined so as to find the frequency of its operation at which the thermal actuator produces maximum displacement. Thus we determined the mechanical resonant frequency of the thermal actuators through simulation for titanium, stainless steel and brass thermal actuators. The thermal actuator has slower operating characteristics since its working depends on rate of heat transfer [8].

### *5.3.1 Modeling and Simulation in ANSYS*

To determine this resonant frequency, the thermal actuator was modeled and depending upon the metal with which the thermal actuator was made up of corresponding material property of the metal used was assigned to the modeled structure through meshing. The following boundary condition was then assigned

1. The contact pads are anchored i.e. the degree of freedom is made zero in all three dimensions.

2. Modal analysis was done so as to determine the resonant frequency for mode1, mode 2 and mode 3 of thermal actuators.

Simulation was carried on for 6%, 7%, 8%, 10%, 20%, 30% and 40% thermal actuators each made up metals like titanium, stainless steel and brass.

*5.3.2 Simulation results*

The figure 5.3, 5.4 and 5.5 describes the resonant frequencies at mode1, mode 2 and mode 3 for all three metal thermal actuators. The figure 5.6, 5.7 and 5.8 describes the X, Y and Z displacement of the 7% titanium thermal actuator at its mode 1 resonant frequency, The figure 5.9, 5.10 and 5.11 each describes the X, Y and Z displacement of the 7% titanium thermal actuator at its resonant frequency corresponding to its mode 2 resonant frequency and The figure 5.12, 5.13 and 5.14 each describes the X, Y and Z displacement of the 7% titanium thermal actuator at its resonant frequency corresponding to mode 3 resonant frequency.

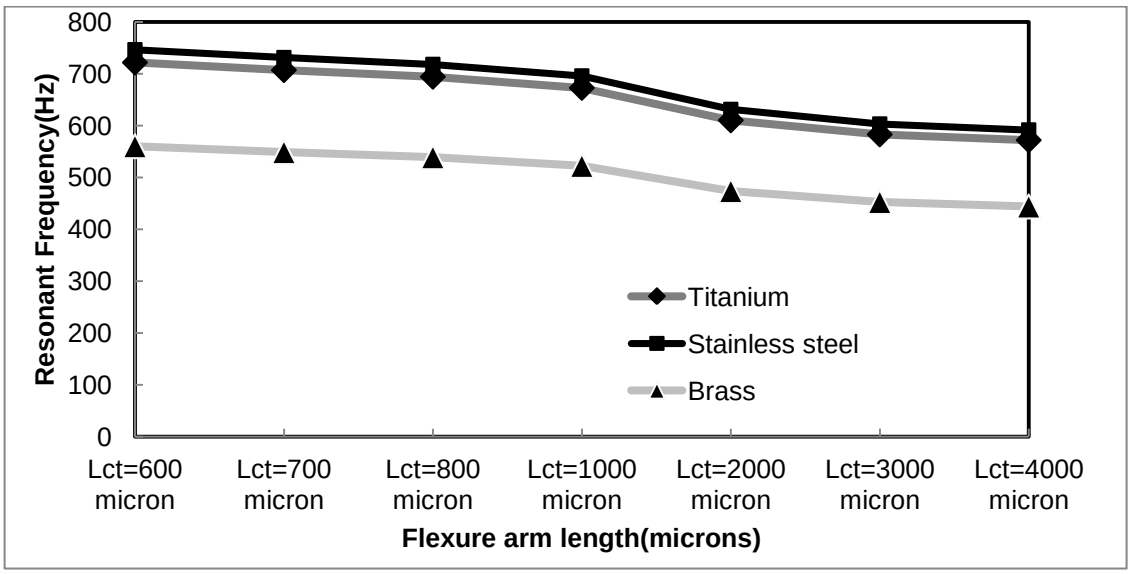


Figure 5.3 Resonant frequencies corresponding to mode 1 for Titanium, Stainless steel and Brass thermal actuators.

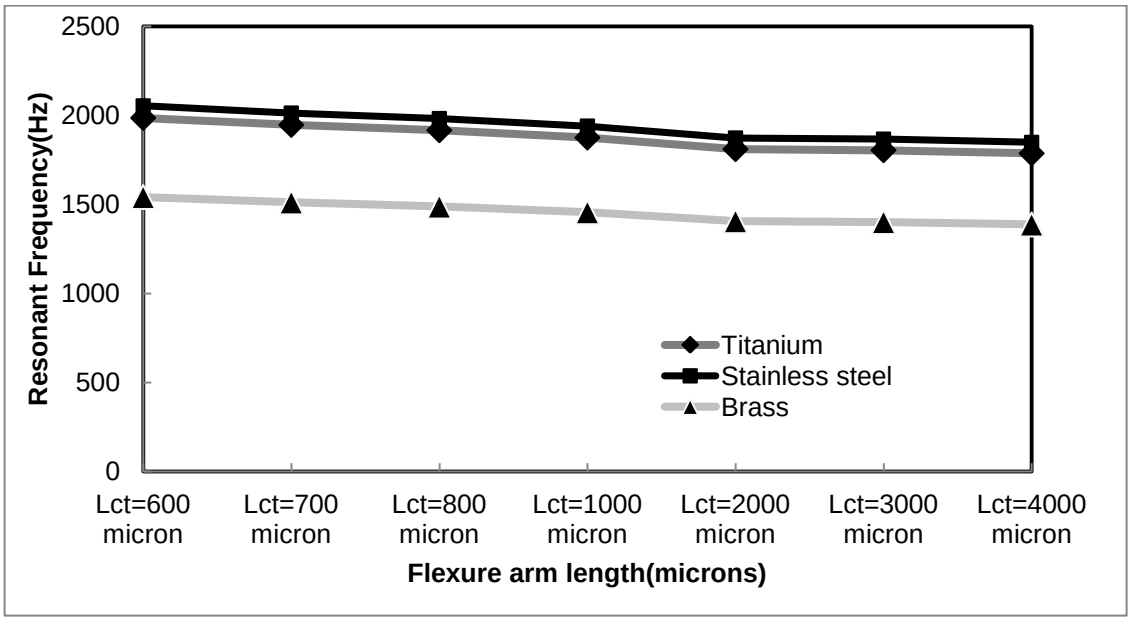


Figure 5.4 Resonant frequencies corresponding to mode 2 for Titanium, Stainless steel and Brass thermal actuators.

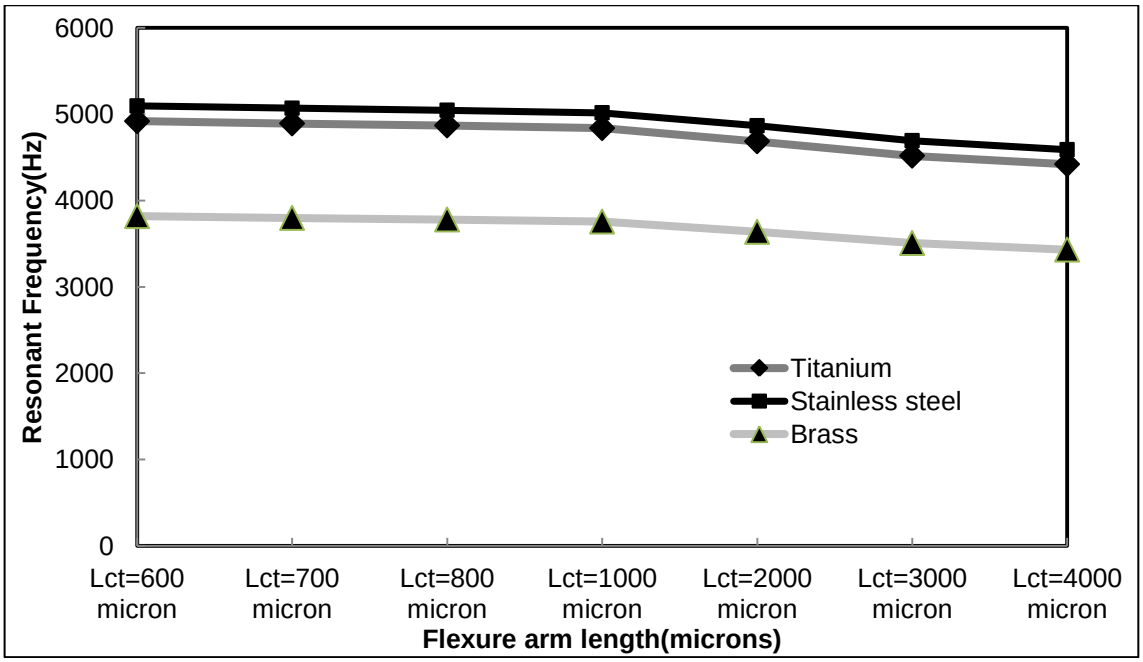


Figure 5.5 Resonant frequencies corresponding to mode 3 for Titanium, Stainless steel and Brass thermal actuators.

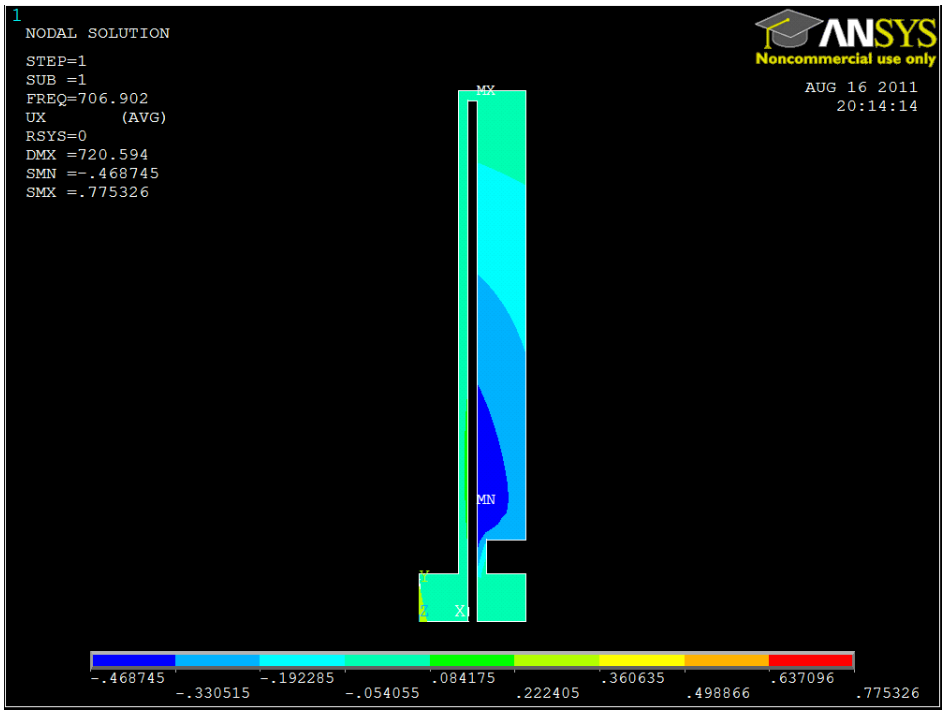


Figure 5.6 X - displacement of 7% Titanium thermal actuator at its mode 1 resonant frequency.

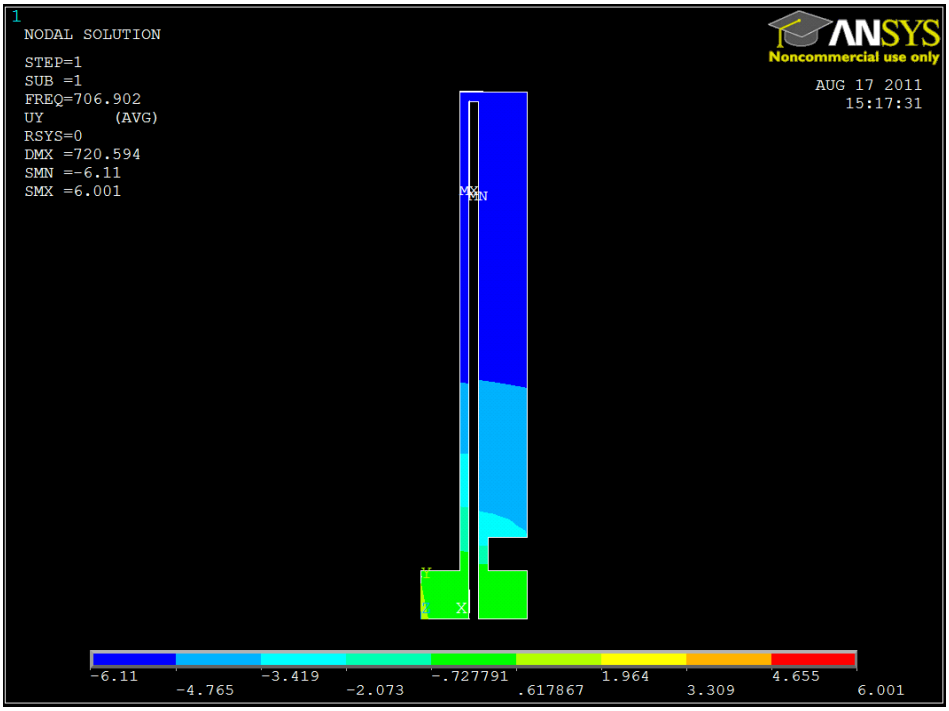


Figure 5.7 Y - displacement of 7% Titanium thermal actuator at its mode 1 resonant frequency.

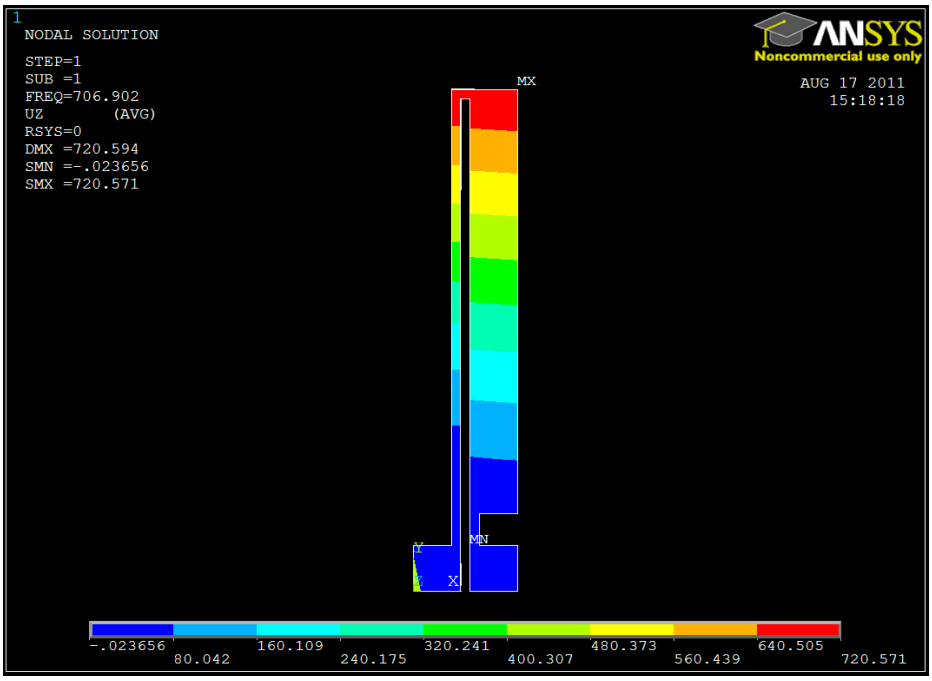


Figure 5.8 Z - displacement of 7% Titanium thermal actuator at its mode 1 resonant frequency.

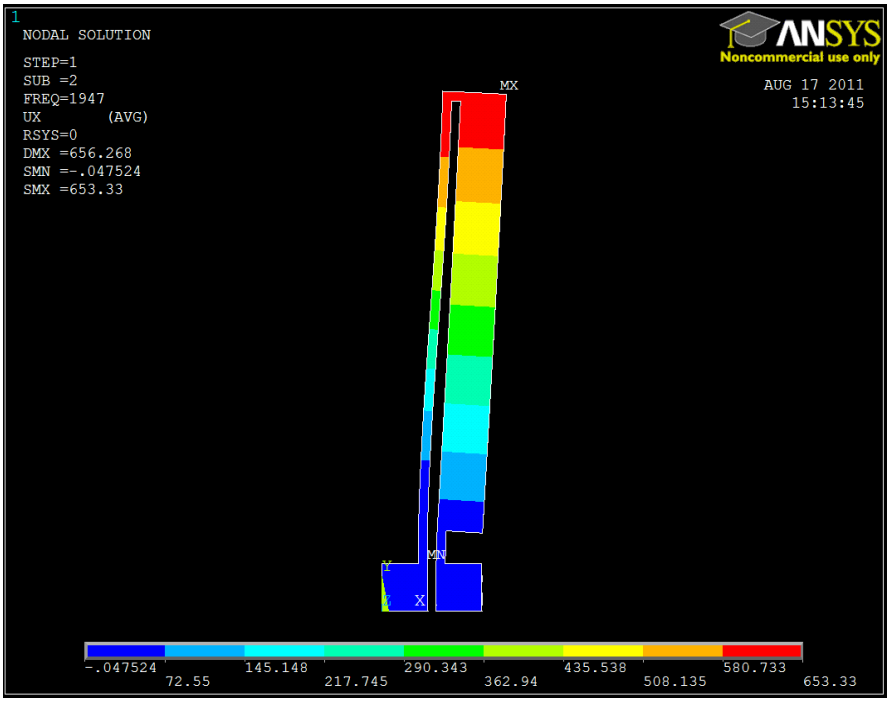


Figure 5.9 X - displacement of 7% Titanium thermal actuator at its mode 2 resonant frequency.

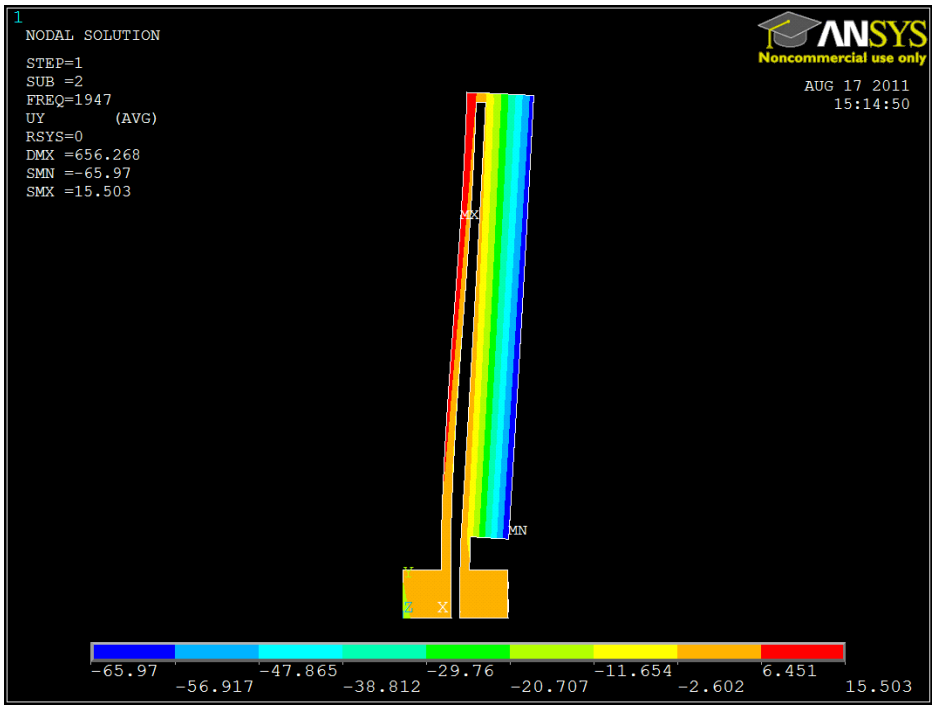


Figure 5.10 Y - displacement of 7% Titanium thermal actuator at its mode 2 resonant frequency.

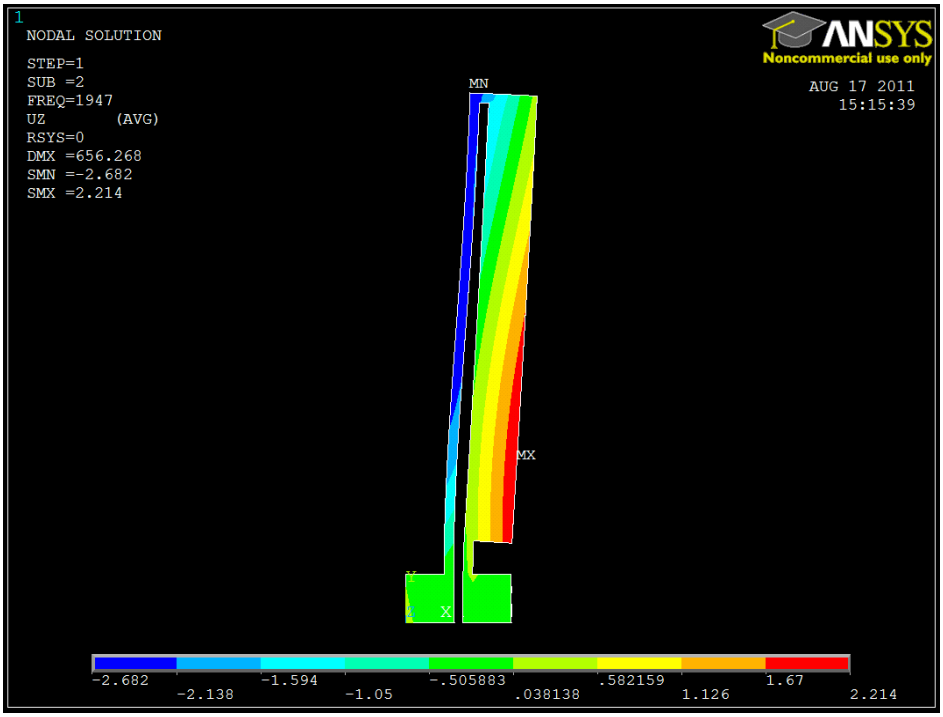


Figure 5.11 Z - displacement of 7% Titanium thermal actuator at its mode 2 resonant frequency.

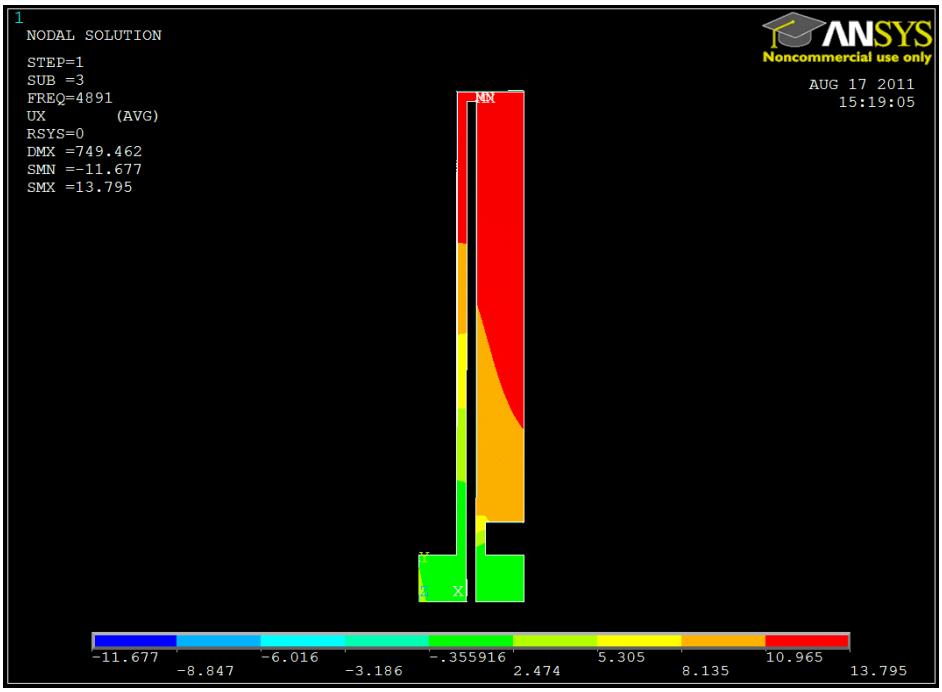


Figure 5.12 X - displacement of 7% Titanium thermal actuator at its mode 3 resonant frequency.

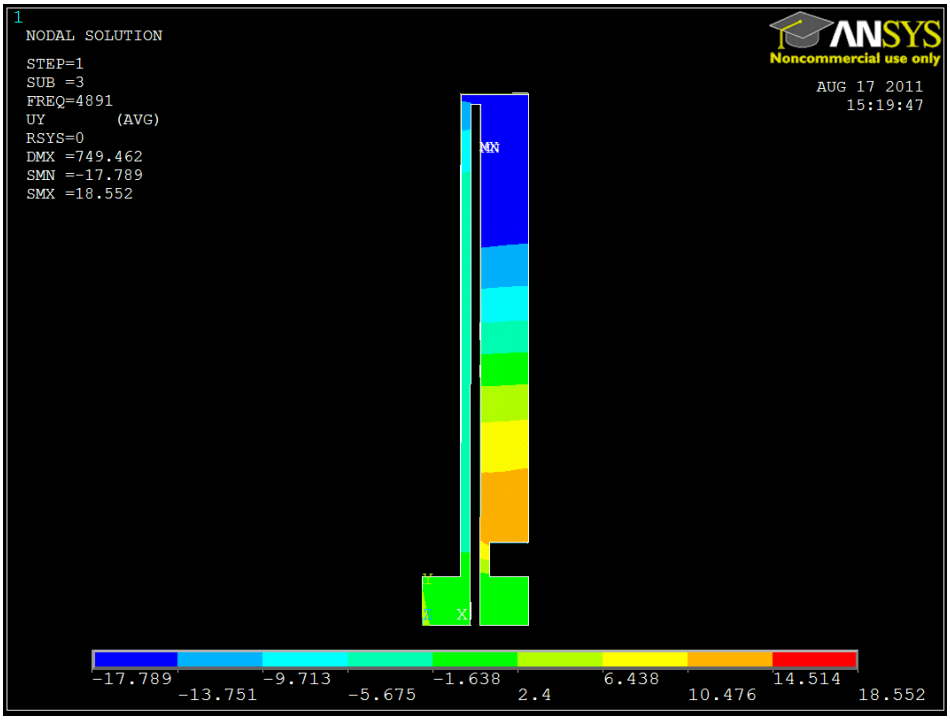


Figure 5.13 Y - displacement of 7% Titanium thermal actuator at its mode 3 resonant frequency.

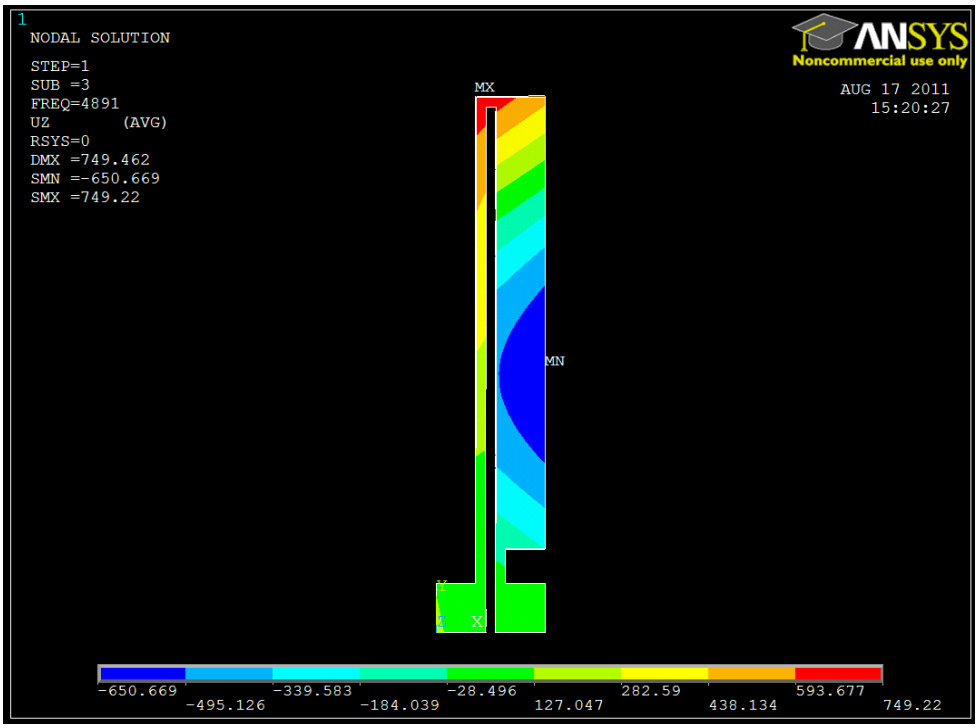


Figure 5.14 Z - displacement of 7% Titanium thermal actuator at its mode 3 resonant frequency.

# CHAPTER 6

# APPLICATION

## 6.1 Introduction

The metal thermal actuators made up of metals like titanium, stainless steel and brass are thus found to produce higher magnitude of displacement and force further it has an improved working current range. The above traits of metal thermal actuators thus help in extending its application platform. In our research we came out with an innovative method of controlling the penetration depth of implantation probe using thermal actuator and also a method to make a body move by harvesting the motion produced by the thermal actuator.

## 6.2 Implantable probes penetration depth control

Implantable probes in brain have been used to study numerous neuro-disorders such as Parkinson's disease, Alzheimer's disease, chronic pain, and addiction by sensing and recording neurotransmitters and extracellular action potential signals. For long term implants, it is important to control the locations of the probe electrodes precisely in tissue in order to receive the signals. We proposed a system design using a metal thermal actuator to control the penetration depth of the implantable probes. The thermal actuators with dimensions of 10×1.4 $mm^2$ and 15×2 $mm^2$ were designed. A multi-electrodes array (MEA) probe based on polyimide substrate was attached vertically on the cold arm of the actuator by heat resistant epoxy. The required force and penetration depth could be precisely achieved by controlling the electric current flowing through the thermal actuator. Experimental results have showed a vertical movement of 1 mm at a current of 1.2 A, indicating our system can be beneficial to control the penetration depth for implantable probes. The figure 6.1 describes the thermal actuator along with implantable probe.

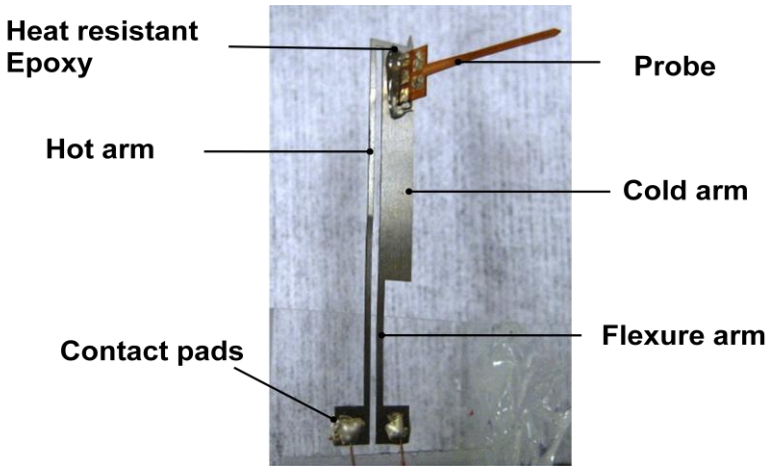


Figure 6.1 Metal thermal actuator with the MEA probe.

## 6.3 Walker

The metal thermal actuator produces an arc like motion and also generates a force of higher magnitude. We utilized the above behavior of metal thermal actuator to come about with an interesting application called walker which uses thermal actuators as a locomotive structure to move itself from one point to another. The figure 6.2 shown below describes the walker.

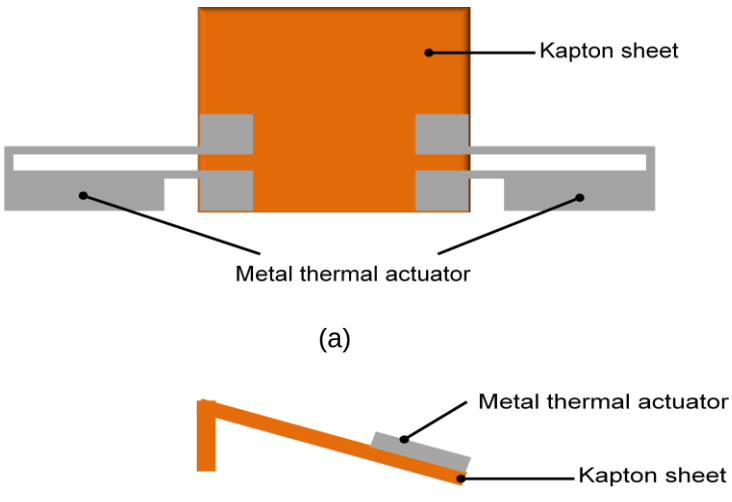


Figure 6.2 Walker (a) Top view (b) Side view.

*6.3.1 Basic principle of working*

The two metal thermal actuators which form the two legs of the walker are placed symmetrically over a rectangular kapton sheet and are attached to the thin kapton sheet with the help of thermal actuator's contact pads using super glue. The kapton sheet forms the body of the walker and was bent at one of its side so that the plane of motion of thermal actuator does not be in parallel with the ground plane over which the walker moves. The basic principle of working was that when the thermal actuator was actuated by passing current, the actuator tip moves and hits the ground platform and lifts the kapton sheet body slightly upwards and pushes it forward thus resulting in the linear motion of the kapton sheet body. The Thermal actuators thus can be actuated by passing current through it at a particular frequency to control the velocity of the walker in motion. Electrically the two thermal actuators are connected in series by connecting their contact pads 2 and 3 with the help of a metal wire, the current are then passed through contact pads 1 and 4 as shown in figure 6.3.

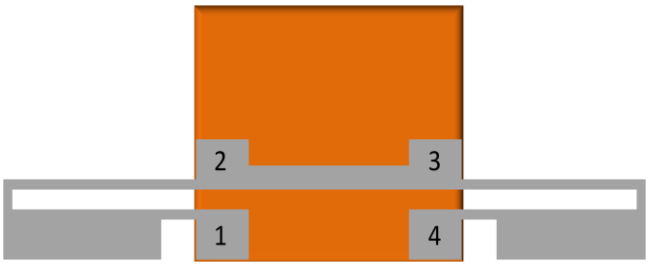


(a)

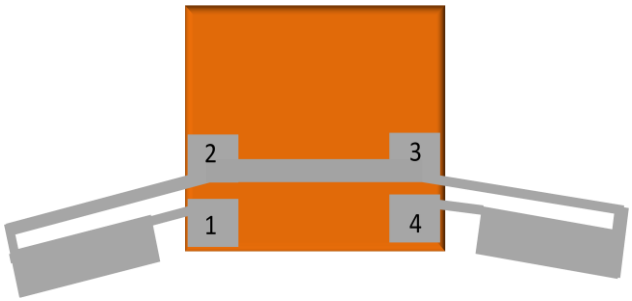


(b)

Figure 6.3 Walker (a) at rest (b) in action.

The figure 6.3 shown above describes the walker at rest, when no current was passed through the thermals actuators and walker in action, when current was passed through the thermal actuators. The figure 6.4 shown below describes the motion of the walker.

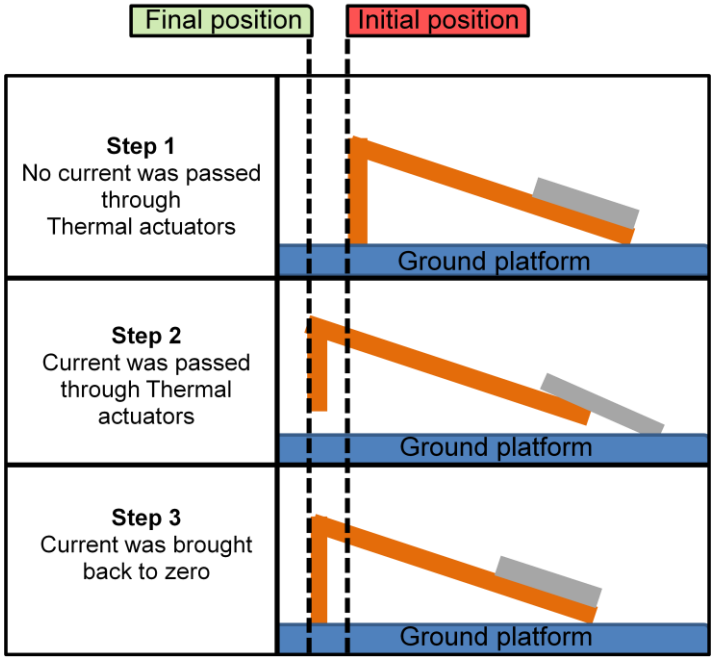


Figure 6.4 Side view on the motion of walker.

*6.3.2 Various phases of walker*

The walker went through the following phases or changes in its design so as to find a suitable method to supply current to the walker's thermal actuators and also to make sure that the method does not impede the motion of the walker. The figure 6.5 describes the phase 1 in the walker's design wherein the current was supplied to the walker by means of copper wires; the copper wires were attached to the contact pads of metal thermal actuator using silver epoxy. We used a thick copper wire first but it was too rigid hence restricted the walker's motion so we replaced it with a thinner copper wire with diameter equivalent to human hair strand but since it

was thinner, it was highly resistive and hence on passing current it melted. The figure 6.6 describes the thicker and thinner copper wire used in phase 1 of walker.

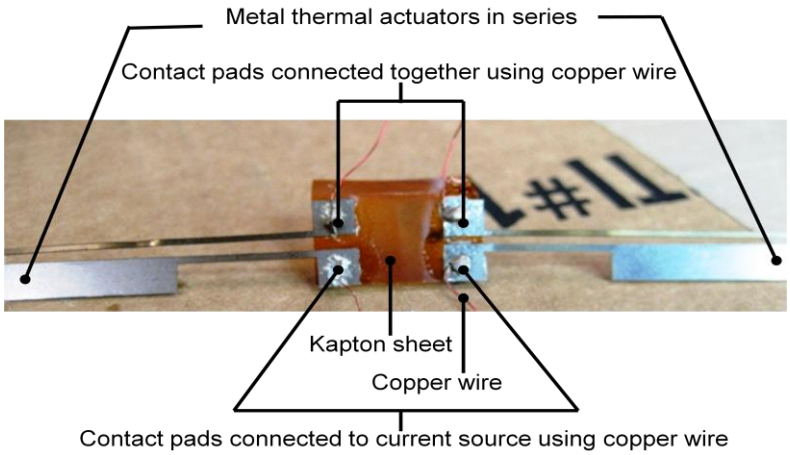


Figure 6.5 Walker phase 1.

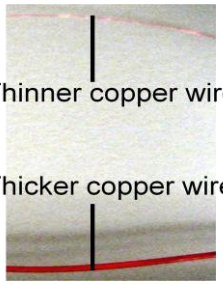


Figure 6.6 Copper wires used in walker phase 1.

The figure 6.7 describes the phase 2 in the walker's design wherein the current was supplied to the walker not by means of copper wires but instead we used two parallel aluminum rails to supply current, one of the two parallel rails was connected to the positive terminal of the current source and the other rail was connected to its negative terminal. The walker now acts as a bridge between the two rails. The design of walker was modified such that we used a two thin metal strip that are connected to contact pads 1 and 4 of the walker as shown in figure 6.7 such that they protrude out from the kapton body and makes contact with the parallel rails.

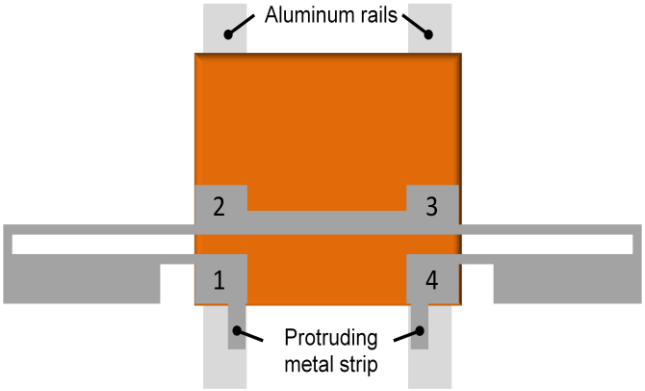


(a)

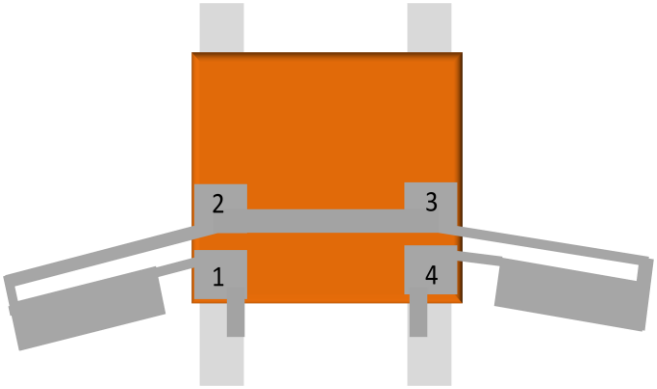


(b)

Figure 6.7 Walker phase 2 (a) at rest (b) in action.

When the walker was at rest, the contact pads 1 and 4 are in contact with the parallel rails through the thin metal strips and when current was passed through the parallel rails, the kapton body of the walker lifts up and moves forward at the same time thus the walker looses its contact with the parallel rails and then slowly the thermal actuator cools down and the walker's kapton body comes down slowly thus again a contact with parallel rails will be established by the walker and this process repeats itself resulting in the linear motion of the walker. The figure 6.8 describes the working of walker phase 2. The figure 6.9 represents the experimental setup and also the top and side view of the walker phase 2.

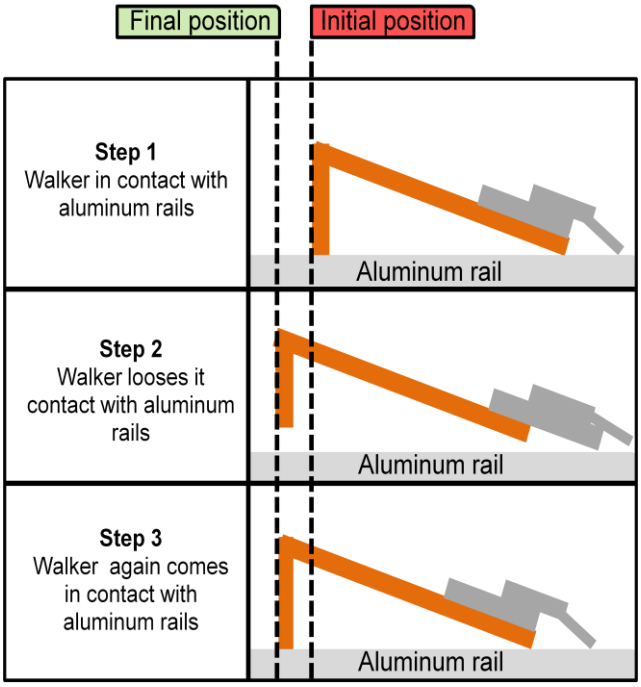


Figure 6.8 Side view on motion of Walker phase 2.

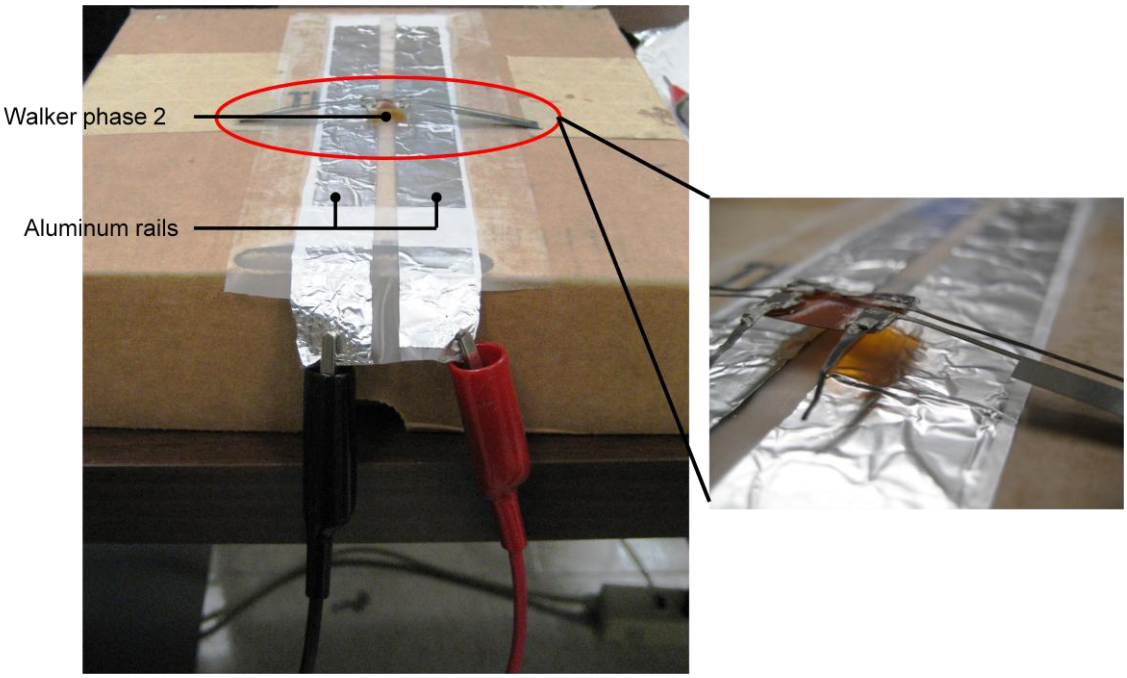


Figure 6.9 Experimental setup of Walker phase 2 with the magnified view of circled region on left in the right hand side.

The figure 6.10 describes the phase 3 in the walker's design wherein the two parallel aluminum rails used in walker phase 2 was replaced by two parallel copper wires and the parallel copper wires was lifted off the ground through poles, one of the two parallel copper wires was connected to the positive terminal of the current source and the other copper wire was connected to its negative terminal. The walker now acts as a bridge between the two copper wires. The design of walker was modified such that we used a two thick copper wires are connected to contact pads 1 and 4 of the walker as shown in figure 6.10 such that they extend upwards in an upright position and makes contact with the two parallel overhead copper wire rails.

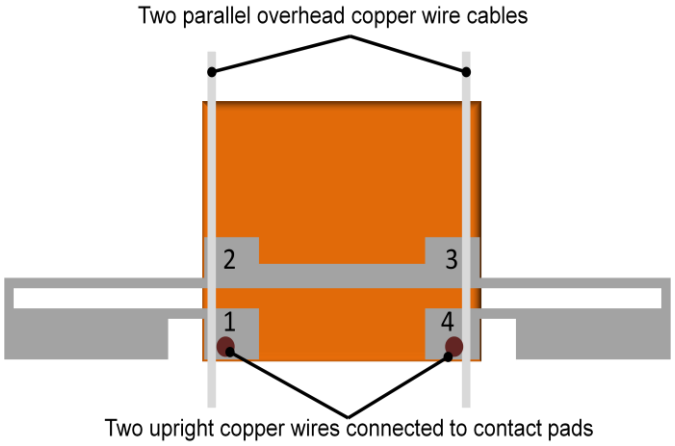


(a)

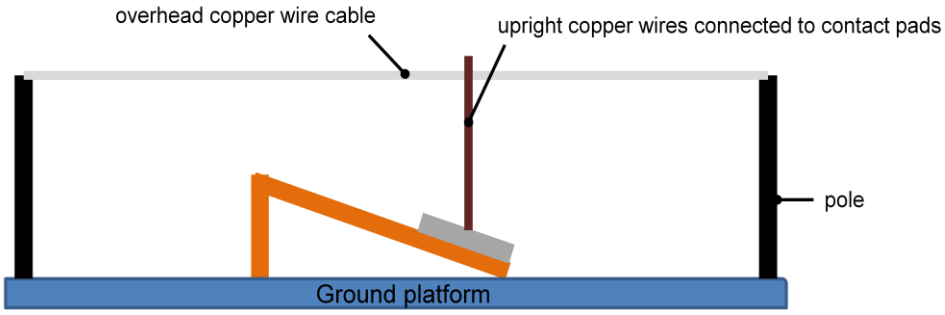


(b)

Figure 6.10 Walker phase 3 (a) Top view (b) Side view.

The figure 6.11 describes the motion of walker phase 3 in a side view perspective and the figure 6.12 represents the experimental setup of walker phase 3.

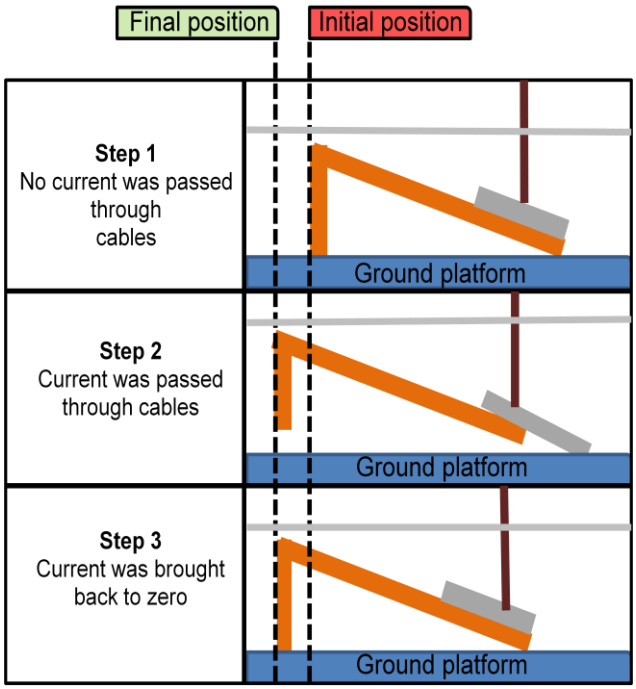


Figure 6.11 Side view on motion of Walker phase 3.

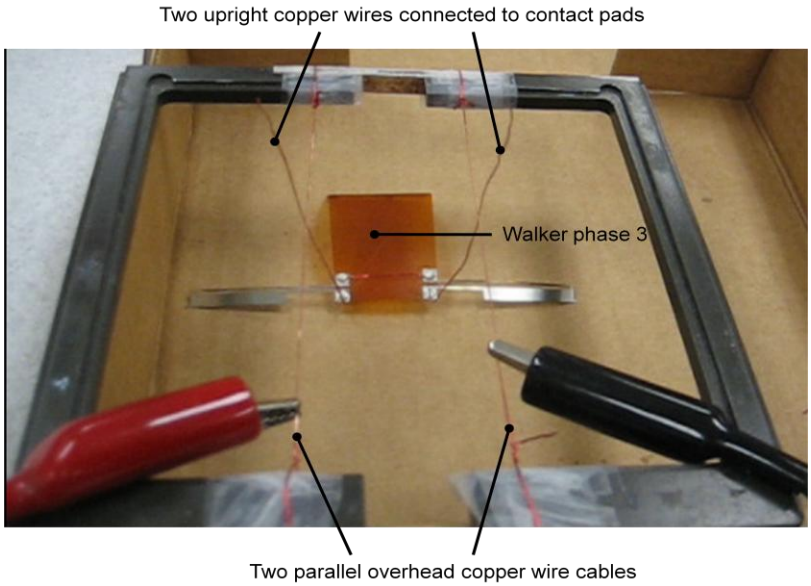


Figure 6.12 Experimental setup of walker phase 3.

REFERENCES

[1] Qing-An Huang and Neville Ka Shek Lee," Analysis and design of polysilicon thermal flexure actuator," *J. Micromech. Microeng,* vol. 9, no. 1, pp. 65-70, March. 1999.

[2] Robert K. Messenger, "Modeling and control of surface micromachined thermal actuators," M.S. thesis, Dept. Mech. Eng., Brigham Young Univ., Utah, USA, 2004.

[3] Dr. Ghantasala, Danielle Simmons and Sudesh Woodiga," The Design and Simulation of a Microcantilever for Microactuator Applications," Mech. and Aeronautical Eng. Dept., Western Michigan Univ., Kalamazoo, MI, Rep. MAE-05-09, 2005.

[4] Michael S. Baker, Richard A. Plass, Thomas J. Headley, Jeremy A. Walraven, "Compliant Thermo-Mechanical MEMS Actuators LDRD #52553," Sandia National Lab., Albuquerque, New Mexico. Rep. SAND2004-6635, 2004.

[5] J. Robert Reid, Victor M. Bright and John H. Comtois, "Force measurements of polysilicon thermal microactuators," Proc. SPIE 2882, 296 (1996); doi10.1117/12.250716.

[6] Kolesar, E.; Htun, T.; Least, B.; Tippey, J.; , "Design and Performance Comparison of Single- and Double-Hot Arm Polysilicon Surface Micromachined Electrothermal Actuators and Arrays Applied to Realize a Microengine," *Nanotechnology, 2008. NANO '08. 8th IEEE Conference on* , vol., no., pp.444-447, 18-21 Aug. 2008.

[7] Geisberger, A.A.; Sarkar, N.; Ellis, M.; Skidmore, G.D.; , "Electrothermal properties and modeling of polysilicon microthermal actuators," *Microelectromechanical Systems, Journal of* , vol.12, no.4, pp. 513- 523, Aug. 2003.

[8] Roberto Venditti, Jacky S H Lee, Yu Sun and Dongqing Li, " An in-plane, bi-directional electrothermal MEMS actuator," *J. Micromech. Microeng,* vol. 16, no. 10, pp. 2067-2070, Oct 2006.

[9] J. Comtois and V. Bright, "Applications for surface-micromachined polysilicon thermal actuators and arrays," Sensors and Actuators A, vol. 58, no. 1, pp. 19-25, 1997.

## BIOGRAPHICAL INFORMATION

Thangamani Balasubramanian Praveen Balaji received his Bachelor"s of Engineering in Electronics and communication Engineering from Anna University, India in 2009. He is pursuing his Master's of Science in Electrical Engineering at the University of Texas at Arlington. His research interests include MEMS based thermal actuators and embedded microcontroller systems. He has published conference papers and posters during his work in the iMEMS laboratory.